

# Low energy excitations and dynamic Dzyaloshinskii-Moriya interaction in $\alpha'$ - $\text{NaV}_2\text{O}_5$ studied by far infrared spectroscopy

T. Rõõm,\* D. Huvonen, and U. Nagel

*National Institute of Chemical Physics and Biophysics, Akadeemia tee 23, 12618 Tallinn, Estonia.*

Y.-J. Wang

*National High Magnetic Field Laboratory, Florida State University,  
1800 East Paul Dirac Drive, Tallahassee, FL 32306*

R. K. Kremer

*Max-Planck-Institut für Festkörperforschung, Heisenbergstraße 1, D-70569 Stuttgart, Germany*

(Dated: June 19, 2018)

(Accepted for publication in Physical Review B)

We have studied far infrared transmission spectra of  $\alpha'$ - $\text{NaV}_2\text{O}_5$  between 3 and  $200\text{ cm}^{-1}$  in polarizations of incident light parallel to  $a$ ,  $b$ , and  $c$  crystallographic axes in magnetic fields up to 33 T. The temperature dependence of the transmission spectra was studied close to and below the phase transition temperature  $T_c = 34\text{ K}$ . The triplet origin of an excitation at  $65.4\text{ cm}^{-1}$  ( $8.13\text{ meV}$ ) is revealed by splitting in the magnetic field. The  $g$ -factors for the triplet state are  $g_a = 1.96 \pm 0.02$ ,  $g_b = 1.975 \pm 0.004$  and  $g_c = 1.90 \pm 0.03$ . The magnitude of the spin gap at low temperatures is found to be magnetic field independent at least up to 33 T. All other infrared-active transitions appearing below  $T_c$  are ascribed to zone-folded phonons. Two different dynamic Dzyaloshinskii-Moriya (DM) mechanisms have been discovered that contribute to the oscillator strength of the otherwise forbidden singlet to triplet transition. *First*, the strongest singlet to triplet transition is an electric dipole transition where the polarization of the incident light's electric field is parallel to the ladder rungs ( $\mathbf{E}_1 \parallel \mathbf{a}$ ). This electric dipole active transition is allowed by the dynamic DM interaction created by a high frequency optical  $a$ -axis phonon. *Second*, in the incident light polarization perpendicular to the ladder planes ( $\mathbf{E}_1 \parallel \mathbf{c}$ ) an enhancement of the singlet to triplet transition is observed when the applied magnetic field shifts the singlet to triplet resonance frequency to match the  $68\text{ cm}^{-1}$   $c$ -axis phonon energy. The origin of the second mechanism is the dynamic DM interaction created by the  $68\text{ cm}^{-1}$   $c$ -axis optical phonon. The strength of the dynamic DM is calculated for both mechanisms using the presented theory.

PACS numbers: 78.30.Hv, 75.10.Pq, 71.70.Gm, 76.30.Fc

## I. INTRODUCTION

The opening of a spin gap is of fundamental interest in one-dimensional spin one-half systems. In one-dimensional Heisenberg spin chains the coupling between the spins and lattice leads to the spin-Peierls instability; the atomic distances change together with the nearest neighbor exchange coupling between the spins. As a result the spin gap opens separating the singlet ground state from the excited triplet state. The spin-Peierls instability was discovered in organic compounds and later on in inorganic  $\text{CuGeO}_3$ <sup>1</sup>. Although  $\alpha'$ - $\text{NaV}_2\text{O}_5$  is another spin one-half quasi-one-dimensional compound where the spin gap opening and the lattice distortion take place simultaneously<sup>2,3</sup>, it is different from canonical spin-Peierls systems. The magnetic field dependence of the phase transition temperature<sup>4,5</sup>  $T_c$  and the entropy change<sup>6</sup> at  $T_c$  are not consistent with the magneto-elastically driven phase transition in  $\alpha'$ - $\text{NaV}_2\text{O}_5$ , where in addition to the displacement of atoms at  $T_c = 34\text{ K}$  a new charge order appears<sup>7,8,9,10</sup>. An extra degree of freedom comes from one electron being shared by the V-O-V rung as  $\alpha'$ - $\text{NaV}_2\text{O}_5$  is a quarter-filled two leg spin ladder compound. In the low temperature phase unpaired elec-

trons on V-O-V rungs shift from the middle of the rung to off-center positions and a zigzag pattern of  $\text{V}^{4+}$  and  $\text{V}^{5+}$  ions along the ladder legs exists on all ladders<sup>7,8,11</sup>. There are four ladder planes in the unit cell at ambient pressure and under high pressure a series of successive phase transitions to phases with more than four planes in the unit cell are observed<sup>12</sup>.

$\alpha'$ - $\text{NaV}_2\text{O}_5$  is not an ideal one-dimensional spin system as revealed by inelastic neutron scattering (INS)<sup>13,14</sup>. In addition to the dispersion of magnetic excitations along the ladder direction two dispersion curves with a rather small dispersion of  $1.2\text{ meV}$  along the ladder rung direction are observed. One curve is at  $8\text{ meV}$  and the other at  $10\text{ meV}$  at the center of the Brillouin zone. More exact spin gap value,  $8.13\text{ meV}$  ( $65.5\text{ cm}^{-1}$ ), has been determined by the high field electron spin resonance<sup>15,16</sup>.

Doubling of the lattice constants along  $a$ - and  $b$ -axes and quadrupling along  $c$ -axis create additional Raman and infrared active modes at the phase transition temperature. The question is whether they are all zone-folded lattice modes or some of them are spin excitations. The controversial modes are infrared active modes polarized along the  $c$ -axis at  $68$  and  $106\text{ cm}^{-1}$  and Raman modes with frequencies nearly matching the fre-

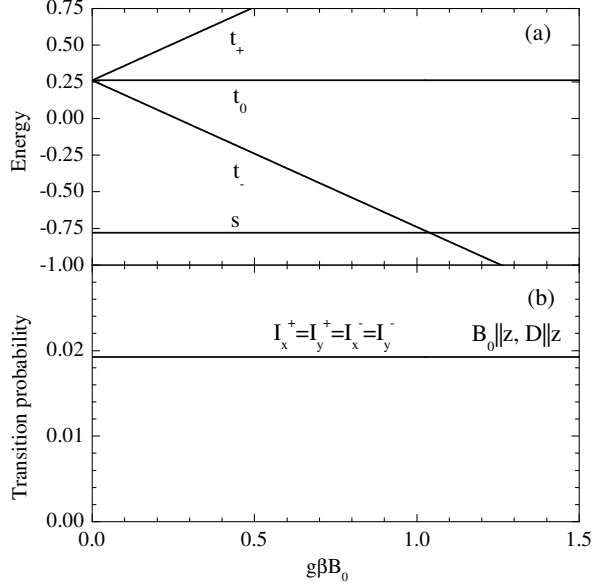


FIG. 1: Two spins coupled by the isotropic exchange coupling,  $J = 1$ , and the DM interaction,  $\mathbf{D} \parallel \mathbf{B}_0$ ,  $D = 0.4$ . (a) – energy levels;  $|t_{-}\rangle = |T_{-}\rangle$  and  $|t_{+}\rangle = |T_{+}\rangle$  are pure triplet states in any field. (b) – non-zero transition probabilities  $I_i^j$  from the ground state  $|s\rangle$  to the triplet state  $|t_j\rangle$  for a given orientations  $i = x$  or  $y$  of the alternating magnetic field  $\mathbf{H}_1$ .

quencies of the two infrared modes. The origin of the 68 and  $106\text{ cm}^{-1}$  excitations is of fundamental interest since the  $68\text{ cm}^{-1}$  excitation is almost degenerate with the  $65.5\text{ cm}^{-1}$  triplet. Spin chain models do not predict a bound singlet excitation being degenerate with the triplet excitation<sup>17,18,19</sup>.

Electric and magnetic dipole transitions between singlet and triplet states are forbidden in principle. The reason for this is the different parity of the ground singlet state and the excited triplet state. The singlet state is anti-symmetric and the triplet state is symmetric relative to the interchange of two spins. Electric dipole or magnetic dipole operators, responsible for the optical absorption, will not couple these two states. An anti-symmetric interaction can mix singlet and triplet states. If such interaction exists the transitions are partially allowed. The strength of the partially allowed optical transition, either magnetic dipole or electric dipole, depends on the orientation of the light polarization and applied magnetic field with respect to the crystal axes. Using infrared spectroscopy it is possible not only to extract a separation of energy levels in a spin system, but also find the origin of the transition, either electric dipole or magnetic dipole, and the orientation of the anti-symmetric interaction.

In this paper we study spin gap excitations and phonons in  $\alpha'\text{-NaV}_2\text{O}_5$  using far-infrared spectroscopy. To explain the experimentally observed singlet to triplet

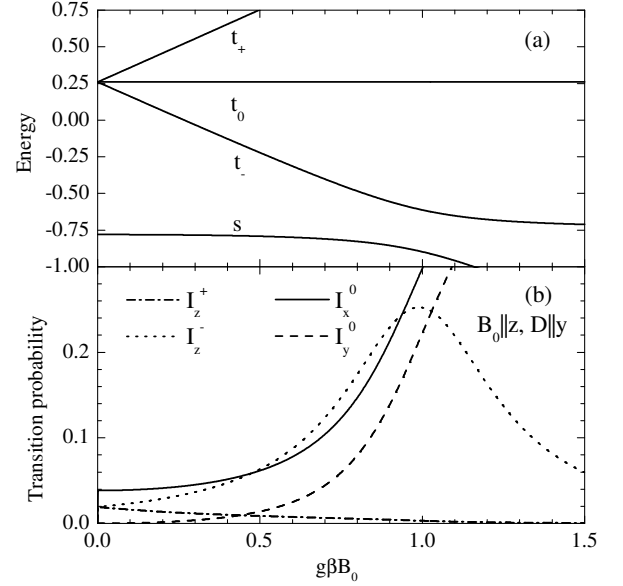


FIG. 2: Two spins coupled by the isotropic exchange coupling,  $J = 1$ , and the DM interaction,  $\mathbf{D} \perp \mathbf{B}_0$ ,  $D = 0.4$ . (a) – energy levels;  $|t_0\rangle = |T_0\rangle$  is a pure triplet state in any field. (b) – non-zero transition probabilities  $I_i^j$  from the ground state  $|s\rangle$  to the triplet state  $|t_j\rangle$  for given orientations  $i = x, y$ , or  $z$  of the alternating magnetic field  $\mathbf{H}_1$ .

absorption we present a calculation of the dynamic Dzyaloshinskii-Moriya (DM) absorption mechanism by numerical diagonalization of the spin-phonon hamiltonian. Analytical results in the perturbation theory for the small dynamic DM interaction are given. Also, the theory of the second relevant mechanism, the magnetic dipole active static DM mechanism is presented.

## II. STATIC AND DYNAMIC DZYALOSHINSKII-MORIYA INTERACTION

The anti-symmetric DM interaction, introduced by Dzyaloshinskii<sup>20</sup> and Moriya<sup>21</sup>, is a combination of superexchange and spin-orbital interactions and is linear in spin-orbital coupling. For a particular spin system the allowed components of the DM interaction are determined by the symmetry of the spin complex<sup>20,21</sup>. Corrections to the energy spectrum due to the DM interaction are usually small because the correction is proportional to  $D^2/\Delta$ , where  $D$  is the magnitude of the DM interaction and  $\Delta$  is the separation of the singlet and triplet energy levels. In addition to the DM interaction there is a symmetric spin-spin interaction that is quadratic in spin-orbital coupling. Although the symmetric interaction does not couple the singlet and triplet states it affects the splitting of the triplet state sublevels. It was shown by Shekhtman *et al.*<sup>22,23</sup> for a single bond superexchange

that the triplet state remains degenerate in zero magnetic field if both symmetric and anti-symmetric spin-spin interactions are taken into account.

Although the corrections to the energy levels are small, the mixing of the singlet and the triplet state by the anti-symmetric interaction could be enough to produce experimentally detectable optical singlet to triplet transitions. The transition probabilities for the magnetic dipole operator in spin chains with DM interactions were calculated by Sakai *et al.*<sup>24</sup>. The idea that the electric dipole singlet to triplet transition is partially allowed when an optically active phonon lowers the crystal symmetry and therefore creates a dynamic DM interaction, was put forward by Cépas *et al.*<sup>25,26</sup>. Below we calculate the energy spectra and transition probabilities using a simple two spin model. In the case of the static DM mechanism the full spin hamiltonian with Shekhtman corrections is used. For the dynamic DM interaction we extend the theory of Cépas *et al.* beyond the perturbation theory and solve the hamiltonian by exact diagonalization.

#### A. Magnetic dipole transitions and Dzyaloshinskii-Moriya interaction for a spin pair

In this section we calculate the energy spectrum and the magnetic dipole transition probabilities for two isotropically exchange coupled spins ( $S = 1/2$ ) in the presence of the anti-symmetric DM interaction and the second-order symmetric interaction. We find the eigenvalues and eigenstates of the hamiltonian  $H = H_0 + H_{sx}$  and calculate the transition probabilities from the ground state induced by the magnetic dipole operator

$$H_{md} = g\mu_B \mathbf{H}_1 \cdot (\mathbf{S}_1 + \mathbf{S}_2), \quad (1)$$

where  $\mathbf{H}_1$  is the magnetic field component of the light,  $g$  is the electron g-factor, and  $\mu_B$  is the Bohr magneton. The zero-order hamiltonian is

$$H_0 = J\mathbf{S}_1 \cdot \mathbf{S}_2 + g\mu_B \mathbf{B}_0 \cdot (\mathbf{S}_1 + \mathbf{S}_2), \quad (2)$$

where  $J$  is the isotropic exchange coupling between spins  $\mathbf{S}_1$  and  $\mathbf{S}_2$ , and  $\mathbf{B}_0$  is the applied static magnetic field. The first and second order corrections are (Eq.(2.19) from Ref.<sup>23</sup>)

$$H_{sx} = -\frac{|\mathbf{D}|^2}{4J}\mathbf{S}_1 \cdot \mathbf{S}_2 + \frac{1}{2J}\mathbf{S}_1 \cdot \mathbf{D}\mathbf{D} \cdot \mathbf{S}_2 + H_{DM}, \quad (3)$$

where  $\mathbf{D}$  is the DM vector and we have separated the anti-symmetric DM interaction

$$H_{DM} = \mathbf{D} \cdot [\mathbf{S}_1 \times \mathbf{S}_2]. \quad (4)$$

We choose singlet and triplet as the basis of eigenstates since they are the eigenstates of  $H_0$ . These states are the singlet  $|\mathbf{S}\rangle = (|+-\rangle - |-+\rangle)/\sqrt{2}$  and the three components of the triplet  $|\mathbf{T}_-\rangle = |--\rangle$ ,  $|\mathbf{T}_0\rangle = (|+-\rangle + |-+\rangle)/\sqrt{2}$ , and  $|\mathbf{T}_+\rangle = |++\rangle$ . The spin quantization axis  $z$  is chosen parallel to the applied field  $\mathbf{B}_0$  and for a single spin  $\langle +|S_z|+\rangle = -\langle -|S_z|-\rangle = 1/2$ . Let the state vector be  $|\Psi\rangle = (T_+, T_0, T_-, S)$ . We diagonalize the hamiltonian  $H = H_0 + H_{sx}$  for two orientations of applied field, along the DM vector and perpendicular to the DM vector, denoting the eigenstates by  $(t_+, t_0, t_-, s)$ .

$\mathbf{B}_0 \parallel \mathbf{D} \parallel \mathbf{z}$ . The hamiltonian in the matrix representation is

$$H = \begin{pmatrix} \frac{1}{4}J + \frac{1}{16}D^2J^{-1} + G_z & 0 & 0 & 0 \\ 0 & \frac{1}{4}J - \frac{3}{16}D^2J^{-1} & -\frac{1}{2}\imath D & 0 \\ 0 & 0 & 0 & \frac{1}{4}J + \frac{1}{16}D^2J^{-1} - G_z \\ 0 & \frac{1}{2}\imath D & 0 & -\frac{3}{4}J + \frac{1}{16}D^2J^{-1} \end{pmatrix}, \quad (5)$$

where  $G_z = g\mu_B B_0$  is the Zeeman term. For arbitrarily chosen  $J = 1$  and  $D = 0.4$  the energy levels are shown in Fig.1(a). The symmetric part of  $H_{sx}$  adds a correction  $D^2/(16J)$  to all energy levels except  $|\mathbf{T}_0\rangle$  where it is  $-3D^2/(16J)$ . This correction for  $|\mathbf{T}_0\rangle$  is partially canceled by  $H_{DM}$  that mixes  $|\mathbf{S}\rangle$  and  $|\mathbf{T}_0\rangle$ . As a result the triplet state sublevels stay degenerate in zero magnetic field as was pointed out in ref.<sup>22,23</sup>. The net effect of  $H_{sx}$  in zero field is to lower the singlet state energy by  $-3D^2/(16J)$  and to raise the triplet state energy by  $D^2/(16J)$ .

The transition probability for the magnetic dipole operator (1) from the ground state is calculated as  $I_i^j = |\langle t_j | S_{1i} + S_{2i} | s \rangle|^2$ ,  $i = x, y, z$ . The alternating magnetic field  $\mathbf{H}_1$  polarized along  $x$  or  $y$  axis (perpendicular to  $\mathbf{B}_0$  and  $\mathbf{D}$ ) gives non-zero intensities as shown in Fig.1(b). This is because  $|s\rangle$  has the triplet component  $|\mathbf{T}_0\rangle$  mixed in and the transitions from  $|\mathbf{T}_0\rangle$  to  $|\mathbf{T}_-\rangle$  and  $|\mathbf{T}_+\rangle$  are allowed by  $S_x$  and  $S_y$  operators. The transition probabilities do not depend on the strength of the applied field since the mixing of  $|\mathbf{S}\rangle$  and  $|\mathbf{T}_0\rangle$  is independent of  $\mathbf{B}_0$ .

$\mathbf{B}_0 \perp \mathbf{D} \parallel \mathbf{y}$ . The hamiltonian is

$$H = \begin{pmatrix} \frac{1}{4}J - \frac{1}{16}D^2J^{-1} + G_z & 0 & -\frac{1}{8}D^2J^{-1} & \frac{\sqrt{2}}{4}D \\ 0 & \frac{1}{4}J + \frac{1}{16}D^2J^{-1} & 0 & 0 \\ -\frac{1}{8}D^2J^{-1} & 0 & \frac{1}{4}J - \frac{1}{16}D^2J^{-1} - G_z & \frac{\sqrt{2}}{4}D \\ \frac{\sqrt{2}}{4}D & 0 & \frac{\sqrt{2}}{4}D & -\frac{3}{4}J + \frac{1}{16}D^2J^{-1} \end{pmatrix}. \quad (6)$$

In this field orientation  $|T_-\rangle$  and  $|T_+\rangle$  are mixed into  $|S\rangle$  by  $H_{DM}$  and  $|t_0\rangle$  remains a pure state,  $|t_0\rangle = |T_0\rangle$ . Note that there is an avoided crossing at  $g\mu_B B_0 \approx 1$  between  $|s\rangle$  and  $|t_-\rangle$  as shown in Fig. 2(a).

The transitions from  $|s\rangle$  to  $|t_-\rangle$  and  $|t_+\rangle$  are observed when  $\mathbf{H}_1 \parallel \mathbf{B}_0$ , see  $I_z^-$  and  $I_z^+$  in Fig. 2(b). In high magnetic field  $I_z^-$  prevails over  $I_z^+$  because the mixing of  $|T_-\rangle$  into the ground state increases and the mixing of  $|T_+\rangle$  decreases. Finite transition probability  $I_x^0$  to the  $|t_0\rangle$  is observed in small fields when  $\mathbf{H}_1 \perp \mathbf{B}_0, \mathbf{D}$  whereas  $I_y^0 = 0$  ( $\mathbf{H}_1 \parallel \mathbf{D}$ ) as  $B_0$  approaches zero. Both transition probabilities are determined by the amount  $|T_-\rangle$  and  $|T_+\rangle$  are mixed into the ground state since transition operators  $S_x$  and  $S_y$  couple these two states to the  $|t_0\rangle = |T_0\rangle$  state.  $I_x^0$  and  $I_y^0$  gain intensity as the ground state changes into  $|T_-\rangle$  with increasing field.

In summary, the following selection rules are observed for the magnetic dipole transition from the singlet to the triplet state in the presence of DM interaction. *First*, if the magnetic field is parallel to the DM vector  $\mathbf{D} \parallel \mathbf{B}_0$ , transitions to the triplet state sublevels  $|t_-\rangle$  and  $|t_+\rangle$  are observed. These transitions have field-independent intensities and do not depend on polarization in the plane perpendicular to the DM vector,  $\mathbf{H}_1 \perp \mathbf{D}$ . *Second*, if the magnetic field is perpendicular to the DM vector  $\mathbf{B}_0 \perp \mathbf{D}$ , then in small fields ( $B_0 \ll J/g\mu_B$ ) the transition to  $|t_0\rangle$  has a weak field dependence and is observed in polarization  $\mathbf{H}_1 \perp \mathbf{B}_0, \mathbf{D}$ . The transitions to  $|t_-\rangle$  and  $|t_+\rangle$  are observed in  $\mathbf{H}_1 \parallel \mathbf{B}_0$  polarization. In this polarization in magnetic fields,  $g\mu_B B_0 \geq D$ , the transition probability to  $|t_-\rangle$  increases and to  $|t_+\rangle$  decreases with increasing field. Sakai *et al.*<sup>24</sup> calculated magnetic dipole transition probabilities for interacting spin chains using a 16 spin cluster. In their model the symmetric anisotropic superexchange was not considered. Our single dimer model leaves the triplet levels degenerate whereas the degeneracy is lifted in their calculation. Whether the degeneracy will be lifted or not when the symmetric anisotropic superexchange in addition to the anti-symmetric DM interaction is included in their model needs a separate study.

## B. Electric dipole transitions and dynamic Dzyaloshinskii-Moriya interaction for a spin pair

We show that the electric field component of the far-infrared light  $\mathbf{E}_1$  that couples to an optically active phonon can cause transitions between singlet and triplet

states if this phonon creates a DM interaction by lattice deformation.

Electric dipole coupling between the phonon and the light in the long wavelength limit is

$$V = eQE_1, \quad (7)$$

where  $e$  is an effective charge associated with a lattice normal coordinate  $Q$ . Here we assume that the electric field is polarized parallel to the electric dipole moment of the normal coordinate  $Q$  and we have dropped the time dependence of  $V$ .

We expand the DM vector  $\mathbf{D}$  into a power series of  $Q$

$$\mathbf{D}(Q) = \mathbf{D}(0) + \frac{\partial \mathbf{D}}{\partial Q} \Big|_{Q=0} Q + \dots \quad (8)$$

The first term is the static DM vector in the absence of lattice deformation. We already demonstrated in the previous section that this interaction gives rise to magnetic dipole transitions between singlet and triplet states. Here for simplicity we take  $\mathbf{D}(0) = 0$ . We will ignore terms quadratic in  $\mathbf{D}$  in  $H_{sx}$  (Eq.3) because these symmetric interactions will not give us any transitions between singlet and triplet states. Leaving out higher order terms of  $Q$  we get for the DM interaction (4)

$$H_{DMQ} = Q\mathbf{D}_Q \cdot [\mathbf{S}_1 \times \mathbf{S}_2], \quad (9)$$

where  $\mathbf{D}_Q \equiv \frac{\partial \mathbf{D}}{\partial Q} \Big|_{Q=0}$ . For the phonon system we use the secondary quantization presentation. The lattice normal coordinate  $Q$  can be presented in terms of creation and annihilation operators  $a^\dagger$  and  $a$ ,  $Q = q(a^\dagger + a)$ , where  $q$  is the transformation coefficient. Since we left out  $Q^2$  and higher order terms in Eq.(8), the dynamic DM interaction will couple two phonon states  $|n\rangle$  and  $|n'\rangle$ , where  $n' = n \pm 1$ ;  $n$  is the occupation number of phonons in mode  $Q$ .

The hamiltonian of the coupled spin-phonon system is

$$H = \hbar\omega_p a^\dagger a + J\mathbf{S}_1 \cdot \mathbf{S}_2 + g\mu_B \mathbf{B}_0 \cdot (\mathbf{S}_1 + \mathbf{S}_2) + H_{DMQ}^{(1)}, \quad (10)$$

$$H_{DMQ}^{(1)} = q(a^\dagger + a)\mathbf{D}_Q \cdot [\mathbf{S}_1 \times \mathbf{S}_2], \quad (11)$$

$\hbar\omega_p$  is the phonon energy. In the low temperature limit  $k_B T \ll \hbar\omega$  the thermal population of phonon states is low,  $\langle n \rangle \approx 0$ , and we can consider only the phonon states with either 0 or 1 phonon,  $|0\rangle$  and  $|1\rangle$ . After diagonalization of the hamiltonian (10) we treat  $V$ , Eq.(7), as a time-dependent perturbation to calculate the transition probabilities from the ground state. We choose  $|S\rangle$  and

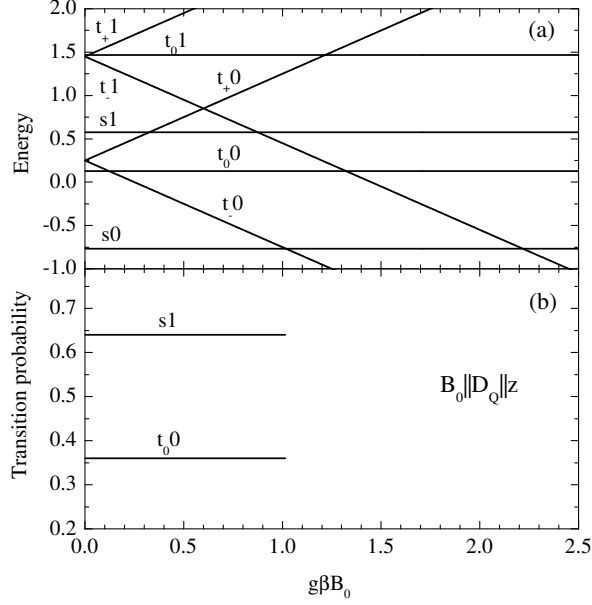


FIG. 3: Two spins coupled by the isotropic exchange coupling,  $J = 1$ , and the dynamic DM interaction,  $qD_Q = 0.4$ , created by the phonon with a frequency  $\hbar\omega_p = 1.2$ ;  $\mathbf{D}_Q \parallel \mathbf{B}_0$ . (a) – energy levels;  $|t_{\pm}0\rangle$  and  $|t_{\pm}1\rangle$  are pure states  $|T_{\pm}0\rangle$  and  $|T_{\pm}1\rangle$  in any field. (b) – non-zero electric dipole transition probabilities from the ground state to the coupled spin-phonon state  $|t_{00}\rangle$  and  $|s1\rangle$ . The graph is not extended above the field where the ground state changes from the singlet  $|s0\rangle$  to the triplet  $|t_{-0}\rangle$ .

$|T_i\rangle$  with the quantization axis along the applied field  $\mathbf{B}_0$  as the basis for the spin states. Let the state vector be  $\Psi = (T_{+1}, T_{+0}, T_{01}, T_{00}, T_{-1}, T_{-0}, S1, S0)$ . The hamiltonian is diagonal in this basis except for the last term,  $H_{DMQ}^{(1)}$ . The eigenstates are labeled by  $|sn\rangle$  and  $|t_{in}\rangle$  where  $n = 0$  or  $1$ . We solve two separate cases,  $\mathbf{D}_Q \parallel \mathbf{B}_0$  and  $\mathbf{D}_Q \perp \mathbf{B}_0$ .

$\mathbf{D}_Q \parallel \mathbf{B}_0 \parallel z$ . In this field orientation  $\mathbf{D}_Q = (0, 0, D_Q)$ . The diagonal elements are the same as in (5) except that the phonon energy  $\hbar\omega_p$  will be added if  $n = 1$ . Beside the diagonal elements the non-zero elements of the hamiltonian (10) are the ones created by  $H_{DMQ}^{(1)}$ :  $\langle S1 | H_{DMQ}^{(1)} | T_{00} \rangle = \langle S0 | H_{DMQ}^{(1)} | T_{01} \rangle = -\langle T_{01} | H_{DMQ}^{(1)} | S0 \rangle = -\langle T_{00} | H_{DMQ}^{(1)} | S1 \rangle = iqD_Q/2$ . The energy levels, calculated for  $J = 1$ ,  $\hbar\omega_p = 1.2$ , and  $qD_Q = 0.4$ , are shown in Fig. 3(a). The largest repulsion is between  $|s1\rangle$  and  $|t_{00}\rangle$ , which are the linear combinations of  $|S1\rangle$  and  $|T_{00}\rangle$ . The other two mixed together states are  $|S0\rangle$  and  $|T_{01}\rangle$  giving us the ground state  $|s0\rangle$  and  $|t_{01}\rangle$ . One has to keep in mind that not only the spin states are mixed, but also the phonon states  $|0\rangle$  and  $|1\rangle$  are mixed. All other 4 states that involve triplet states  $|T_{\pm}\rangle$  are pure states.

The splitting of energy levels has to be taken with some

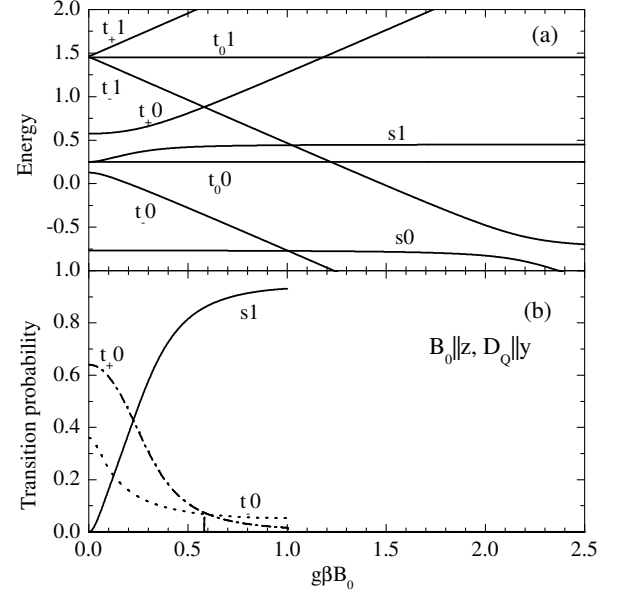


FIG. 4: Two spins coupled by the isotropic exchange coupling,  $J = 1$ , and the dynamic DM interaction,  $qD_Q = 0.4$ , created by the phonon with a frequency  $\hbar\omega_p = 1.2$ ;  $\mathbf{D}_Q \perp \mathbf{B}_0$ . (a) – energy levels;  $|t_{00}\rangle$  and  $|t_{01}\rangle$  are pure states  $|T_{00}\rangle$  and  $|T_{01}\rangle$  in any field. (b) – non-zero electric dipole transition probabilities from the ground state to the coupled spin-phonon state  $|t_{-0}\rangle$  (dotted),  $|t_{+0}\rangle$  (dash-dotted), and  $|s1\rangle$  (solid). The graph is not extended above the field where the ground state changes from the singlet  $|s0\rangle$  to the triplet  $|t_{-0}\rangle$ .

precaution. The splitting due to the dynamic DM is observed when there is one phonon excited,  $n = 1$ . This is not the case at thermal equilibrium at low T when  $\langle n \rangle = 0$  (the possible role of zero-point vibrations is ignored in our approach). If the phonon is brought to the state  $n = 1$  by the light-phonon interaction (7) the effect of one phonon on the shift of energy levels should be observed in the experiment, unless it is much smaller than the lifetime or inhomogeneous broadening of energy levels. The magnitude of the shift and whether it could be observed in the experiment or not will not affect conclusions about the transition probabilities.

Calculation of the transition probability  $|\langle t_j n' | V | s0 \rangle|^2$  is straightforward since  $V$  couples states that are diagonal in the basis of pure spin states and non-diagonal in the basis of phonon states  $|0\rangle$  and  $|1\rangle$ . Two transitions from the ground state  $|s0\rangle$  are observed, to  $|s1\rangle$  and  $|t_{00}\rangle$ , shown in Fig. 3(b). If the dynamic DM is zero, then  $|s0\rangle = |S0\rangle$ ,  $|s1\rangle = |S1\rangle$ , and  $|t_{00}\rangle = |T_{00}\rangle$ . The transition from  $|s0\rangle$  to  $|s1\rangle$  is an ordinary absorption of an infrared photon  $\hbar\omega_p = E_{s1} - E_{s0}$  with probability 1, and the transition to  $|t_{00}\rangle$  has zero probability. When the dynamic DM interaction is turned on, additional absorption sets in and a photon of energy  $E_{t_{00}} - E_{s0}$  is absorbed. This can be viewed as a virtual excitation of a phonon by

the light to the state  $|1\rangle$  while the spin state remains singlet, and then the dynamic DM interaction (9) brings the (virtual) phonon back to  $|0\rangle$  while changing the spin state to  $|T_0\rangle$ . The polarization of the absorbed photon with respect to the crystal axes is determined by the phonon states involved.

$\mathbf{D}_Q \perp \mathbf{B}_0 \parallel \mathbf{z}$ . We take  $\mathbf{D}_Q = (0, D_Q, 0)$ . Beside diagonal elements there are 8 non-zero elements  $\langle T_{+1}|H_{DMQ}^{(1)}|S_0\rangle$ ,  $\langle T_{+0}|H_{DMQ}^{(1)}|S_1\rangle$ ,  $\langle T_{-1}|H_{DMQ}^{(1)}|S_0\rangle$ ,  $\langle T_{-0}|H_{DMQ}^{(1)}|S_1\rangle$ ,  $\langle S_1|H_{DMQ}^{(1)}|T_{+0}\rangle$ ,  $\langle S_1|H_{DMQ}^{(1)}|T_{-0}\rangle$ ,  $\langle S_0|H_{DMQ}^{(1)}|T_{+1}\rangle$ ,  $\langle S_0|H_{DMQ}^{(1)}|T_{-1}\rangle$ , all equal to  $\sqrt{2}qD_Q/4$ . The energy levels, calculated for  $J = 1$ ,  $\hbar\omega_p = 1.2$ , and  $qD_Q = 0.4$ , are plotted in Fig. 4(a).

The strongest mixing occurs between  $|S_1\rangle$  and  $|T_{\pm 0}\rangle$  giving the eigenstates  $|s_1\rangle$  and  $|t_{\pm 0}\rangle$ . Also, there is an additional mixing between  $|T_{-0}\rangle$  and  $|T_{+0}\rangle$  levels in small fields.

In small fields,  $g\mu_B B_0 < J$ , the mixing of  $|S_0\rangle$  and  $|T_{\pm 1}\rangle$  is less pronounced since their separation is larger than the separation of  $|S_1\rangle$  and  $|T_{\pm 0}\rangle$ . Therefore, for the analysis of the transition probabilities the ground state can be taken as pure  $|S_0\rangle$  and the transition probabilities are mainly determined by the mixing between  $|S_1\rangle$  and  $|T_{\pm 0}\rangle$ . The effect of mixing of  $|T_{\pm 1}\rangle$  into the ground state has a secondary effect on the transition probabilities. Transitions from the ground state to three excited states  $|t_{+0}\rangle$ ,  $|t_{-0}\rangle$ , and  $|s_1\rangle$  have non-zero probabilities (see Fig. 4(b)). The transition probability to the  $|s_1\rangle$  state increases with field because  $|s_1\rangle$  changes gradually from the mixed state into  $|S_1\rangle$ . The transition probabilities to  $|t_{+0}\rangle$  and  $|t_{-0}\rangle$  state decrease as the field increases because the amount of  $|S_1\rangle$  mixed into them decreases. Again, the polarization of the absorbed photon with respect to the crystal axes is determined by the phonon states involved.

*Perturbation theory.* Analytical results can be obtained in the limit  $|E_{S_1} - E_{T_i 0}| \gg qD_Q$ ,  $i = -, 0, +$ . This case holds when  $|\hbar\omega_p - (J \pm g\mu_B B_0)| \gg qD_Q$ . We find the first order perturbation corrections to the states  $|Sn\rangle$  and  $|T_in\rangle$ , where  $n = 0, 1$ , using  $H_{DMQ}^{(1)}$ , Eq. (11), as perturbation. Then the transition probabilities are calculated between the new states  $|s_0\rangle$  and  $|t_i 0\rangle$  as was done in the exact treatment.

For  $\mathbf{D}_Q \parallel \mathbf{B}_0 \parallel \mathbf{z}$  we get

$$|\langle t_0 0|V|s_0\rangle|^2 = I_p \frac{(qD_Q)^2(\hbar\omega_p)^2}{[(\hbar\omega_p)^2 - J^2]^2}, \quad (12)$$

where  $I_p = (eqE_1)^2$  is the light absorption intensity by the infrared-active phonon. The transition probability from  $|s_0\rangle$  to the triplet level  $|t_0\rangle$  is independent of the magnetic field.

For the perpendicular case,  $\mathbf{D}_Q \perp \mathbf{B}_0 \parallel \mathbf{z}$

$$|\langle t_{-0}|V|s_0\rangle|^2 = I_p \frac{(qD_Q)^2(\hbar\omega_p)^2}{2[(\hbar\omega_p)^2 - (J - g\mu_B B_0)^2]^2}, \quad (13)$$

$$|\langle t_{+0}|V|s_0\rangle|^2 = I_p \frac{(qD_Q)^2(\hbar\omega_p)^2}{2[(\hbar\omega_p)^2 - (J + g\mu_B B_0)^2]^2}. \quad (14)$$

If  $\hbar\omega_p \ll J$  then the intensity of the transition from  $|s_0\rangle$  to  $|t_{-0}\rangle$  increases with the magnetic field and decreases for the transition to  $|t_{+0}\rangle$ . If  $\hbar\omega_p \gg J$  then the intensity of the  $|s_0\rangle$  to  $|t_{+0}\rangle$  transition increases and of  $|s_0\rangle$  to  $|t_{-0}\rangle$  decreases. In the perturbation limit the zero field intensities of the transitions from  $|s_0\rangle$  to  $|t_{-0}\rangle$  and  $|t_{+0}\rangle$  are equal.

*In summary*, the following selection rules are obtained for the electric dipole transition from the singlet to the triplet state in the presence of the dynamic DM interaction. **1.** The polarization of the transition:  $\mathbf{E}_1$  is parallel to the dipole moment of the optically active phonon that creates the dynamic DM interaction. **2.** The orientation of the dynamic DM vector  $\mathbf{D}_Q$  is determined by the symmetry of the lattice distortion created by the optically active phonon. **3.** If  $\mathbf{B}_0 \parallel \mathbf{D}_Q$  a magnetic field independent transition probability to the triplet state sublevel  $|t_0 0\rangle$  is observed. **4.** If  $\mathbf{B}_0 \perp \mathbf{D}_Q$  magnetic field dependent transition probabilities to the triplet state sublevels  $|t_{+0}\rangle$  and  $|t_{-0}\rangle$  are observed.

### III. EXPERIMENTAL

We studied several single crystals of  $\alpha'$ - $\text{Na}_x\text{V}_2\text{O}_y$  from the batch E106<sup>27</sup>. According to the heat capacity measurements these crystals have  $T_c = 33.9\text{ K}$ , and the chemical composition  $x = 1.02$  and  $y = 5.06$ . The (ab)-plane properties,  $\mathbf{E}_1 \perp \mathbf{c}$ ,  $\mathbf{k} \parallel \mathbf{c}$ , were studied on three single crystals,  $600\text{ }\mu\text{m}$  (area in the (ab)-plane  $21\text{ mm}^2$ ),  $120\text{ }\mu\text{m}$  ( $20\text{ mm}^2$ ) and  $40\text{ }\mu\text{m}$  ( $3.5\text{ mm}^2$ ) thick in  $\mathbf{c}$ -direction. The (bc)-plane properties,  $\mathbf{E}_1 \perp \mathbf{a}$ ,  $\mathbf{k} \parallel \mathbf{a}$ , were measured on a mosaic of three crystals, each approximately  $650\text{ }\mu\text{m}$  thick, with a total area of  $19\text{ mm}^2$  in the (bc)-plane. The (ac)-plane properties,  $\mathbf{E}_1 \perp \mathbf{b}$ ,  $\mathbf{k} \parallel \mathbf{b}$ , were measured on a mosaic of 7 crystals, each approximately  $800\text{ }\mu\text{m}$  thick, with a total area of  $8.5\text{ mm}^2$  in the (ac)-plane.

The far-infrared measurements were done with a polarizing Martin-Puplett Fourier transform spectrometer<sup>28</sup>. Light pipes were used to guide the far infrared light into the sample cryostat equipped with a 12 T Oxford Instruments magnet and two silicon bolometers from Infrared Laboratories operated at 0.3 K. A rotatable polarizer was mounted at the end of the light pipe in front of the sample to control the polarization of light. Spectra were recorded at 0.2 to  $0.3\text{ cm}^{-1}$  resolution. The magnetic field was applied parallel to the direction of light propagation (Faraday configuration,  $\mathbf{k} \parallel \mathbf{B}_0$ ) or perpendicular to the light propagation (Voigt configuration,  $\mathbf{k} \perp \mathbf{B}_0$ ). Measurements above 12 T were performed at the National High Magnetic Field Laboratory on a 33 T Bitter magnet in the Faraday configuration using a Bruker IFS 113v infrared spectrometer and a 4 K silicon bolometer from Infrared Laboratories.

The anisotropic power absorption coefficient  $\alpha_i(\omega)$  ( $i = a, b, c$ ) was calculated from the measured transmission  $T_i(\omega)$  assuming one back reflection from the crystal front face and one from the back face,  $T_i(\omega) =$

TABLE I: Absorption line positions  $\omega_0$  ( $\text{cm}^{-1}$ ), full widths at half maximum  $\gamma$  ( $\text{cm}^{-1}$ ), and areas ( $\text{cm}^{-2}$ ) in 4.4 K and 40 K spectra of  $\alpha'$ - $\text{NaV}_2\text{O}_5$  in zero magnetic field. Index  $T$  refers to the singlet to triplet excitation and  $F$  to the Fano line shape.

	4.4 K			40 K		
	$\omega_0$	$\gamma$	Area	$\omega_0$	$\gamma$	Area
$\mathbf{E}_1 \parallel \mathbf{a}$	65.4 $T$	0.6	6	90.7 $F$	0.8	120
	91.2	0.2	50			
	101.4	0.26	110			
	101.7	0.19	47			
	111.7	0.18	8			
	126.7	0.17	240			
	127.5	0.22	140			
	138.5	0.4	450			
	140	4.4	2000			
	145.6	0.5	230			
	147.8	0.8	650			
	157.1	0.29	25			
	168.2	0.35	16			
$\mathbf{E}_1 \parallel \mathbf{b}$	25.3	0.55	54	168.6	0.6	20
	26.4	0.47	37			
	30.8	0.84	130			
	32.5	1.05	145			
	34.5	0.95	109			
	36.4	1.51	181			
	65.4 $T$	0.2	0.3			
	39.1	0.43	9			
	91.3	0.3	5			
	101.4	0.24	70			
	111.7	0.2	24			
	126.7	0.26	100			
	127.5	0.2	320			
	145.7	0.58	11			
	148.0	0.65	25			
	168.3	0.42	27			
	180					
	199.4	1.4	157			
	215.1	2.2	420			
$\mathbf{E}_1 \parallel \mathbf{c}$	65.4 $T$	0.2	0.5	214.9	2.5	450
	68	< 1	> 100			
	106	< 2.5	> 110			
	124	< 1	> 50			
	126	< 1.5	> 30			
	130	< 1	> 20			
	132	< 2	> 50			

$(1 - R_i)^2 \exp[-\alpha_i(\omega)d]$ , where  $d$  is the thickness of the crystal. We used a frequency independent value for the reflectance coefficient  $R_i = [(n_i - 1)/(n_i + 1)]^2$ . Indexes of refraction,  $n_i$ , at 4K and terahertz frequencies are  $n_a = 3.64$ ,  $n_b = 3.16$  and  $n_c = 2.70$  (Ref.<sup>29</sup>). According to another paper<sup>30</sup> indexes of refraction at 4K and  $0.55 \text{ cm}^{-1}$  are  $n_a = 3.07$ ,  $n_b = 3.19$  and  $n_c = 2.03$ . We calculated  $n_a/n_b = 1.16$  from the fringe pattern in the 10 to  $50 \text{ cm}^{-1}$  range using our transmission data. This ratio is more similar to the ratio  $n_a/n_b = 1.15$  from Ref.<sup>29</sup> and therefore we used their values for refraction indexes. The real part of the conductivity in units of  $\Omega^{-1} \text{ cm}^{-1}$  is

$$\sigma_1^i(\omega) = n_i(\omega)\alpha_i(\omega)/(120\pi), \quad (15)$$

where in the limit of weak absorption we take  $n_i$  to be independent of frequency.

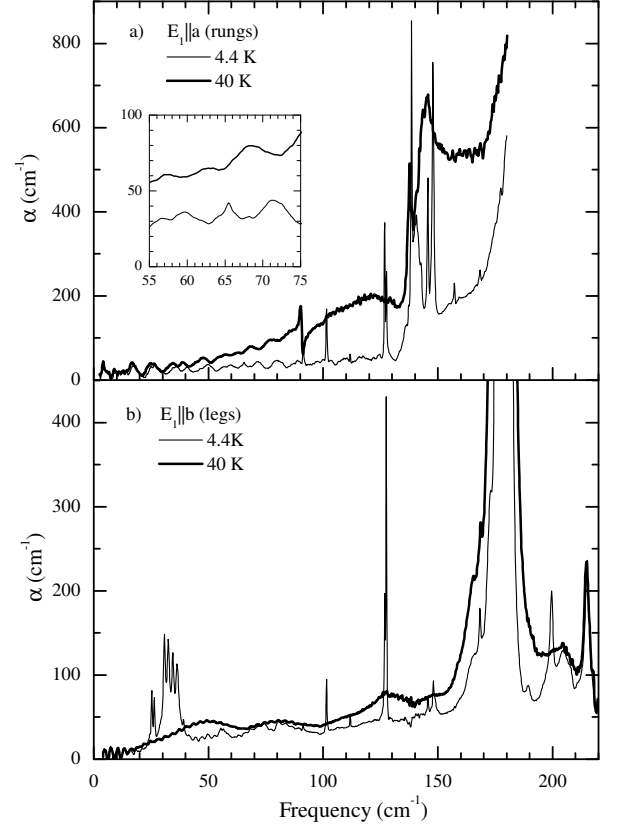


FIG. 5: Absorption spectra of  $\alpha'$ - $\text{NaV}_2\text{O}_5$  below,  $T = 4.4 \text{ K}$ , and above,  $T = 40 \text{ K}$ , the phase transition temperature. (a) –  $\mathbf{E}_1 \parallel \mathbf{a}$ , (b) –  $\mathbf{E}_1 \parallel \mathbf{b}$ . The inset shows the singlet to triplet excitation at  $65 \text{ cm}^{-1}$ .

## IV. RESULTS

### A. Absorption spectra and their temperature dependence

The absorption spectra at temperatures above and below the phase transition temperature  $T_c$  for incident light polarizations  $\mathbf{E}_1 \parallel \mathbf{a}$  and  $\mathbf{E}_1 \parallel \mathbf{b}$  are shown in Fig. 5 and for  $\mathbf{E}_1 \parallel \mathbf{c}$  in Fig. 6. Below  $T_c$  several new lines appear. The line parameters are listed in Table I. The full width at half maximum (FWHM) of the narrowest lines is determined by the used instrument resolution,  $0.2 \text{ cm}^{-1}$ . The best fit for the resolution limited narrow lines was obtained using gaussian line shapes, otherwise a lorentzian line shape was used.

The  $\mathbf{E}_1 \parallel \mathbf{a}$  absorption at 40 K is dominated by a continuous absorption steadily increasing towards high frequencies. Above  $180 \text{ cm}^{-1}$  the absorption is too strong and our data is not reliable above this frequency. There are two derivative-like absorption lines, one at  $91.2 \text{ cm}^{-1}$  and the other at  $140 \text{ cm}^{-1}$ , the latter being relatively broad and has its phase opposite to the  $91.2 \text{ cm}^{-1}$  line

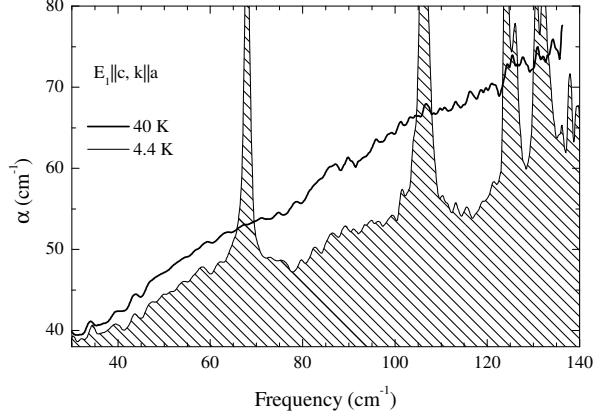


FIG. 6: Absorption spectra at 4.4 K and 40 K in  $\mathbf{E}_1 \parallel \mathbf{c}$  polarization.

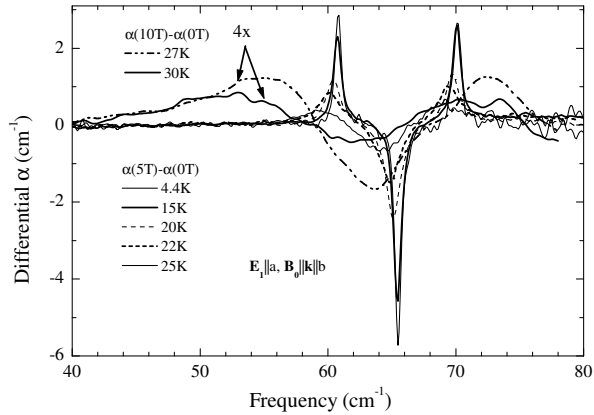


FIG. 7: Temperature dependence of the singlet to triplet absorption spectrum in  $\mathbf{E}_1 \parallel \mathbf{a}$  polarization.

phase. There is a narrow line at  $137.6 \text{ cm}^{-1}$  on top of the  $140 \text{ cm}^{-1}$  line. When  $T$  is lowered, the absorption continuum is diminished over the entire frequency range. Still, substantial absorption continuum remains above  $130 \text{ cm}^{-1}$ . At  $T = 4 \text{ K}$  the  $91.2$  and  $140 \text{ cm}^{-1}$  lines have a normal absorption-like line shape. New lines appear as well: doublets at  $102$ ,  $127$ ,  $147 \text{ cm}^{-1}$  and single lines at  $112$ ,  $157$ ,  $168 \text{ cm}^{-1}$ . The inset in Fig. 5(a) shows a weak line at  $65.4 \text{ cm}^{-1}$ , the singlet to triplet excitation. The magnetic properties of this transition are described in more detail in section IV B. The  $T$  dependent spectra of the singlet to triplet transition are plotted in Fig. 7. To better extract this relatively weak line the difference of two spectra at fixed  $T$ , one measured in  $0 \text{ T}$  field and the other measured in  $5$  or  $10 \text{ T}$  field, was calculated. One can see that the negative line, representing the zero field spectrum, together with the positive features (the lines in  $5$  or  $10 \text{ T}$  spectra) shift to lower frequencies as

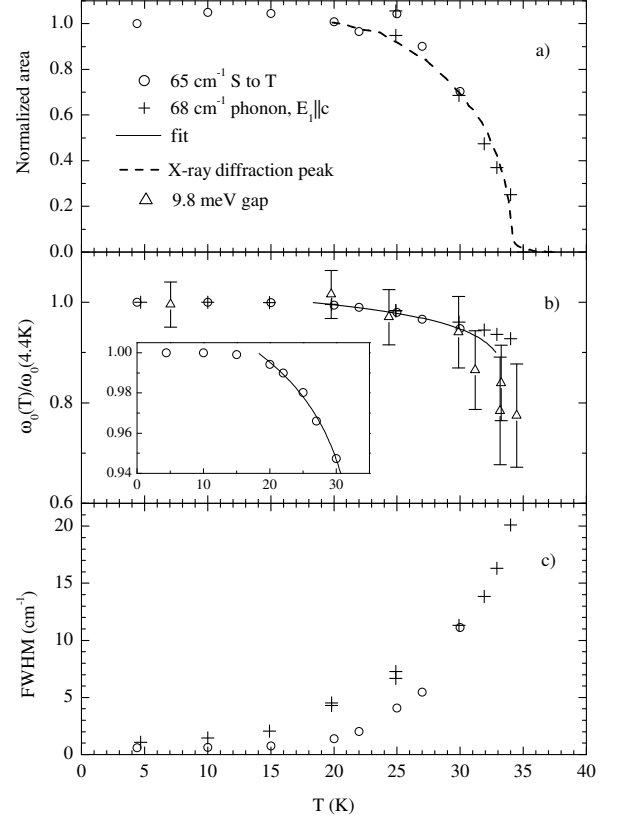


FIG. 8: Zero magnetic field temperature dependence of the normalized absorption line area (panel a), normalized resonance frequency (b), and FWHM (c) for the singlet to triplet transition at  $65.4 \text{ cm}^{-1}$   $\mathbf{E}_1 \parallel \mathbf{a}$  (circles), and for the  $68 \text{ cm}^{-1}$  c-axis phonon (crosses). Inset to (b): the solid line is a fit of the S to T transition energy  $\Delta(T)/\Delta(4.7\text{K}) = (1 - T/T_c)^\beta$  above  $20 \text{ K}$ ;  $T_c = 33.9 \text{ K}$ ,  $\beta = 0.039 \pm 0.002$ . Additionally the X-ray diffraction peak intensity from Ref.<sup>38</sup> is plotted with a dashed line in panel (a) and the normalized gap at  $9.8 \text{ meV}$  measured by INS<sup>3</sup> is shown with triangles in (b).

the temperature increases and at the same time the lines lose intensity and broaden. The temperature dependence of line parameters is plotted in Fig. 8.

The  $\mathbf{E}_1 \parallel \mathbf{b}$  absorption at  $40 \text{ K}$  is dominated by a strong phonon line at  $180 \text{ cm}^{-1}$  and a weaker line at  $215 \text{ cm}^{-1}$ , Fig. 5(b). The temperature-dependent absorption continuum, as was observed in  $\mathbf{E}_1 \parallel \mathbf{a}$  polarization, is absent in  $\mathbf{E}_1 \parallel \mathbf{b}$  (note the different vertical scales in Fig. 5a and 5b). Several lines, at  $101.4$ ,  $111.7$ ,  $126.7$ , and  $127.5 \text{ cm}^{-1}$ , have the same frequency as in the a-axis spectrum, although different strength. The line parameters are listed in Table I. The temperature evolution of the multiplet of seven lines in the  $\mathbf{E}_1 \parallel \mathbf{b}$  spectrum below  $40 \text{ cm}^{-1}$  is shown in more detail in Fig. 9. Below  $T_c = 34 \text{ K}$  a broad line appears at  $32 \text{ cm}^{-1}$ . Another line appears at  $26 \text{ cm}^{-1}$  as  $T$  is lowered. At low  $T$  those two features split into a doublet and a quintet. The line at the highest fre-



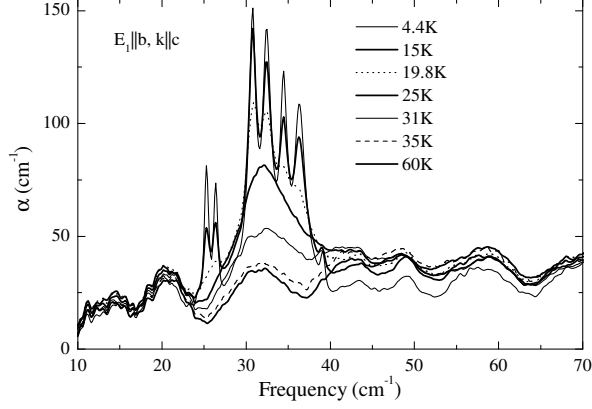


FIG. 9: Temperature dependence of seven low frequency b-axis phonons.

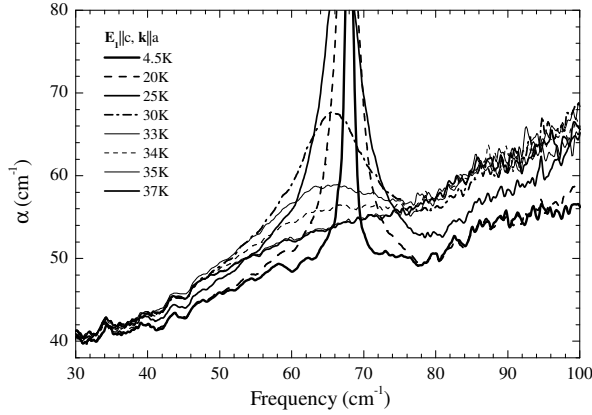


FIG. 10: The temperature dependence of the  $68\text{ cm}^{-1}$  c-axis phonon absorption spectrum.

quency,  $39\text{ cm}^{-1}$ , is relatively weak compared to other six lines. The spectra shown in Fig. 9 have not been corrected for light interference fringes in the sample. The  $60\text{ K}$  spectrum could be used as a background, but with some precaution as some intensity is lost between  $40$  and  $70\text{ cm}^{-1}$  when  $T$  is lowered.

The  $\mathbf{E}_1 \parallel \mathbf{c}$  absorption spectrum has no sharp features below  $140\text{ cm}^{-1}$  in the high temperature phase at  $T = 40\text{ K}$  (Fig. 6). When  $T$  is lowered below  $34\text{ K}$  new lines evolve at  $68$ ,  $106\text{ cm}^{-1}$ , and two doublets around  $124$  and  $132\text{ cm}^{-1}$ . Since the low  $T$  transmission was too small at the transmission minimums and the absorption coefficient cannot be determined accurately, only the upper limits for the line widths and the lower limits for the line areas are given in the Table I. The temperature dependence of the  $68\text{ cm}^{-1}$  line is shown in Fig. 10. The line shifts to lower frequency and broadens as  $T$  is raised from  $4.5\text{ K}$ . Some intensity change is still observed above

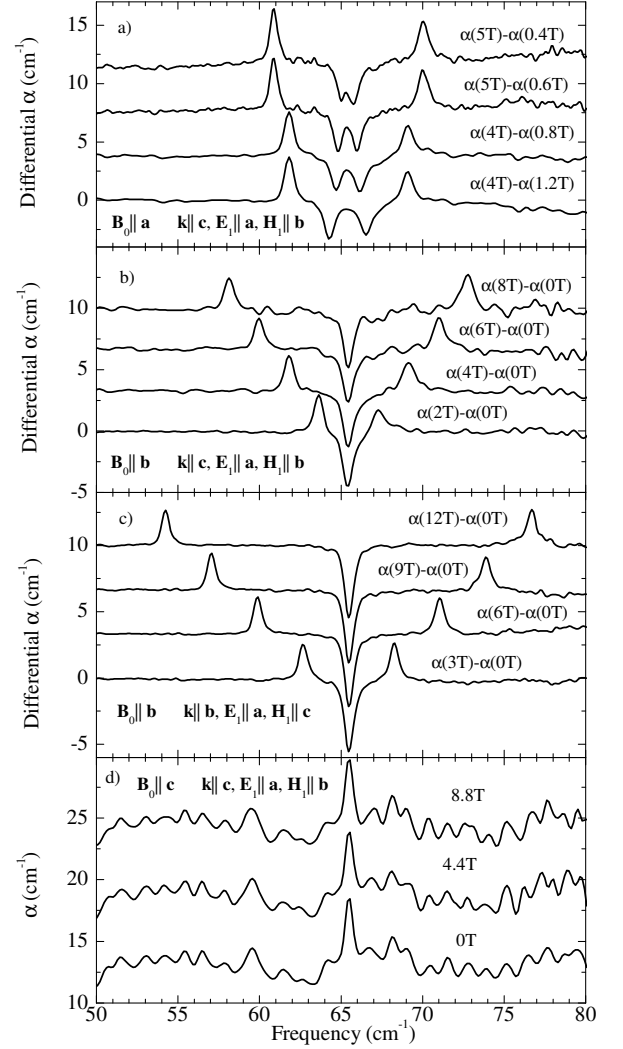


FIG. 11: Magnetic field dependence of the singlet to triplet transition spectra in  $\mathbf{E}_1 \parallel \mathbf{a}$  polarization. Spectra have been shifted in vertical direction. Measurements were done in Voigt (a, b) and in Faraday configuration (c, d).

$T_c$  between  $34$  and  $35\text{ K}$ , but there are no visible differences between the  $35\text{ K}$  and  $37\text{ K}$  spectra. The temperature dependence of line parameters is plotted in Fig. 8 together with the singlet to triplet resonance data. Since the largest experimentally detectable absorption was limited by the thickness of available crystals the line area has been reliably determined only above  $25\text{ K}$ . Below  $25\text{ K}$  the plotted FWHM is the upper limit for the line width.

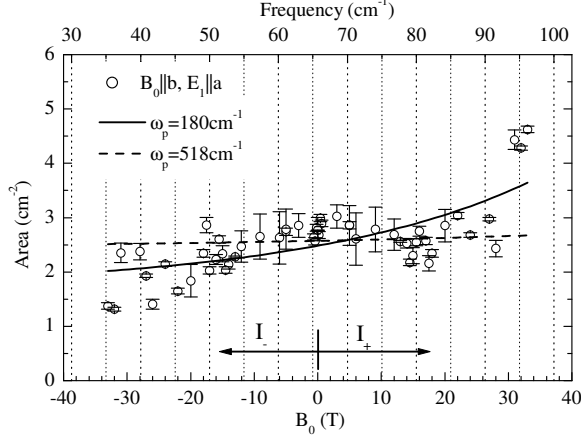


FIG. 12: The magnetic field,  $\mathbf{B}_0 \parallel \mathbf{b}$ , dependence of the singlet to triplet resonance line area at 4.4 K in  $\mathbf{E}_1 \parallel \mathbf{a}$  polarization. The values for the transition to  $m_S = -1$  are plotted in the negative field direction and for the transition to  $m_S = 1$  in the positive field direction;  $g_a \mu_B = 0.922 \text{ cm}^{-1}/\text{T}$ . The lines show the theoretical transition probability for the electric dipole transition for a set of parameters where  $\omega_p$  is the resonance frequency of an optical phonon coupled to the spin system by the dynamic DM interaction: solid line -  $\omega_p = 180 \text{ cm}^{-1}$ , dashed line -  $\omega_p = 518 \text{ cm}^{-1}$ .

### B. Singlet to triplet absorption in magnetic field

We studied the magnetic field effect on the absorption spectra below  $130 \text{ cm}^{-1}$  at 4.4 K in magnetic fields up to 12 T in all three polarizations,  $\mathbf{E}_1 \parallel \mathbf{a}$ ,  $\mathbf{E}_1 \parallel \mathbf{b}$ , and  $\mathbf{E}_1 \parallel \mathbf{c}$ . We did not see any line shifts nor intensity changes except for the  $65.4 \text{ cm}^{-1}$  absorption line.

For  $\mathbf{E}_1 \parallel \mathbf{a}$  polarization the magnetic field effect on the  $65.4 \text{ cm}^{-1}$  line is demonstrated in Fig. 11. When the field  $\mathbf{B}_0$  is parallel to the a- or b-axis, the line splits (panels (a), (b), and (c)). In  $\mathbf{B}_0 \parallel \mathbf{c}$  configuration the line does not split or change its intensity (panel (d)). From the field dependence of the resonance frequency the  $65.4 \text{ cm}^{-1}$  absorption line can be identified as a transition from a singlet ground state,  $S = 0$ , to a triplet excited state,  $S = 1$ . Light is absorbed, depending on its polarization, either by transitions to  $m_S = 1$  and  $m_S = -1$  triplet levels when  $\mathbf{B}_0 \perp \mathbf{c}$  or to the magnetic field independent  $m_S = 0$  level when  $\mathbf{B}_0 \parallel \mathbf{c}$ . The measurements were extended to 33 T in one polarization and field orientation,  $\mathbf{E}_1 \parallel \mathbf{a}$ ,  $\mathbf{B}_0 \parallel \mathbf{b}$ . The field dependence of the singlet to triplet transition line areas is shown in Fig. 12. The lines were fitted with a lorentzian function, full width at half maximum (FWHM) being between  $0.5$  and  $0.6 \text{ cm}^{-1}$ . The line areas of the transitions to the  $m_S = -1$  and  $m_S = 1$  levels depend weakly on the magnetic field. Below (see section V A 1) we calculate the electric dipole transition probability using the presented theory of the dynamic DM effect, and compare it to our measurement results.

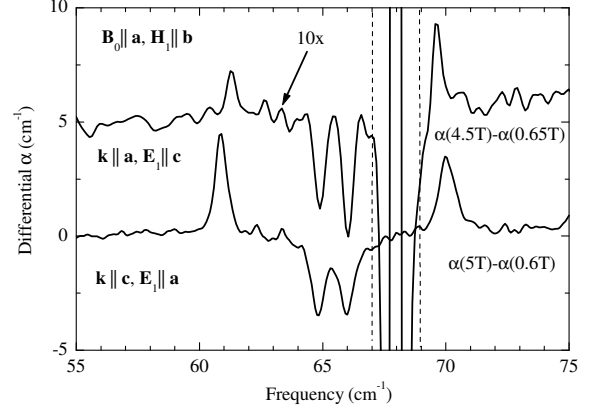


FIG. 13: Differential absorption spectra of the singlet to triplet transition at 4.4 K in  $\mathbf{E}_1 \parallel \mathbf{a}$  and  $\mathbf{E}_1 \parallel \mathbf{c}$  polarizations. The  $\mathbf{E}_1 \parallel \mathbf{c}$  spectrum has been multiplied by 10 and offset in the vertical direction. Both spectra have been measured in  $\mathbf{B}_0 \parallel \mathbf{a}$ ,  $\mathbf{H}_1 \parallel \mathbf{b}$  geometry.

An important question to answer is which component of light,  $\mathbf{E}_1$  or  $\mathbf{H}_1$ , interacts with the spin system. What is common for the data presented in Fig. 11 is that all these measurements were done with the light polarized along the ladder rungs,  $\mathbf{E}_1 \parallel \mathbf{a}$ . We made complementary measurements rotating the incident light's polarization by  $90^\circ$ , thus interchanging the orientations of  $\mathbf{E}_1$  and  $\mathbf{H}_1$ , and found that the singlet to triplet transition was at least ten times weaker if  $\mathbf{E}_1 \perp \mathbf{a}$ . While the data presented in Fig. 11 panels (a), (b), and (d) still leaves open the possibility that the singlet to triplet transition could be a magnetic dipole transition where  $\mathbf{H}_1 \parallel \mathbf{b}$ , there are two other observations that contradict this. *First*, in Fig. 11 (c)  $\mathbf{H}_1$  is not parallel to the b-axis while  $\mathbf{E}_1$  is still parallel to the a-axis and the transition is still strong. *Second*, in Fig. 13 two spectra with  $\mathbf{H}_1 \parallel \mathbf{b}$  are presented for the  $\mathbf{B}_0 \parallel \mathbf{a}$  applied magnetic field orientation. The upper curve with  $\mathbf{E}_1 \parallel \mathbf{c}$  shows about 10 times weaker absorption on the singlet to triplet transition than the lower curve with  $\mathbf{E}_1 \parallel \mathbf{a}$ . Since the same orientation of  $\mathbf{H}_1$  gives different intensities the orientation of magnetic field component of light is irrelevant. Summarizing the results presented in Fig. 11 and 13 we conclude that the strongest contribution to the singlet to triplet absorption comes from an electric dipole transition with the dipole moment along the a-axis.

There are other contributions to the singlet to triplet absorption, although much weaker than in  $\mathbf{E}_1 \parallel \mathbf{a}$  polarization, as is shown in Fig. 13. The upper spectrum is for the c-axis polarized light. Two vertical dashed lines mark the area where the strong absorption due to the  $68 \text{ cm}^{-1}$  excitation takes place in this polarization (see also Fig. 6). One can see that the absorption lines closer to the  $68 \text{ cm}^{-1}$  excitation are stronger than the lines further away.

The line areas measured in different geometries as a function of magnetic field strength are plotted in Fig. 14. We used the method of differential absorption, where spectra taken in different magnetic fields are subtracted from each other to detect weak transitions. In this differential method the transition from the singlet state to the  $m_S = 0$  triplet state escapes detection (unless the intensity depends on the field) since the energy of this triplet level does not change with magnetic field. Therefore, only the intensities of the transitions to the  $m_S = -1$  and  $m_S = 1$  triplet levels can be detected and are plotted in Fig. 14. An interesting finding is the enhancement of the singlet to triplet transition in  $\mathbf{E}_1 \parallel \mathbf{c}$  polarization close to the  $68 \text{ cm}^{-1}$  excitation. It is natural to associate the oscillator strength of this weak transition with the interaction between the spins and the  $68 \text{ cm}^{-1}$  excitation, which has a dipole moment along the c-axis. The exception is  $\mathbf{B}_0 \parallel \mathbf{b}$  orientation where there is no enhancement in  $\mathbf{E}_1 \parallel \mathbf{c}$  polarization. In this field direction only the transition to the  $m_S = 0$  level has a non-zero oscillator strength but is not detected because of the measurement method.

Besides the strong  $\mathbf{E}_1 \parallel \mathbf{a}$  absorption and the resonantly enhanced  $\mathbf{E}_1 \parallel \mathbf{c}$  absorption there is a field-independent oscillator strength, as is seen in Fig. 14(a). No polarization anisotropy is observed there in contrary to the first two mechanisms of singlet to triplet transitions that can be recognized by their polarization dependence. In high fields the transitions to the  $m_S = -1$  and  $m_S = 1$  levels have the same strength in  $\mathbf{E}_1 \parallel \mathbf{b}$  and  $\mathbf{E}_1 \parallel \mathbf{c}$  polarizations (Fig. 14(a)). When  $\mathbf{B}_0 \parallel \mathbf{c}$  and  $\mathbf{E}_1 \parallel \mathbf{b}$  (Fig. 14(b)) the intensity of the transitions to the  $m_S = -1$  and  $m_S = 1$  levels is zero and in this configuration the transition to the  $m_S = 0$  level is active. More detailed analysis of this mechanism is given in V A 3 where we associate this with a magnetic dipole transition.

Within the error limits the g-factors of the triplet state are the same for the two in-plane field orientations  $g_a = 1.97 \pm 0.02$ ,  $g_b = 1.975 \pm 0.004$ . The fit of the resonance frequencies of the singlet to triplet transition for the third field orientation,  $\mathbf{B}_0 \parallel \mathbf{c}$ , gives  $g_c = 1.90 \pm 0.03$ .

In zero field the triplet levels  $m_S = -1, 0$ , and  $1$  are degenerate; it is best seen when comparing the zero field line positions in Fig. 11(c) and (d). Determining the size of the zero field splitting is limited by the linewidth. We can say that the zero field splitting of the triplet levels is less than half of the linewidth,  $\text{FWHM}/2 = 0.25 \text{ cm}^{-1}$ .

## V. DISCUSSION

### A. Triplet state and Dzyaloshinskii-Moriya interaction

In this section we analyze three different contributions to the singlet to triplet optical absorption observed experimentally in  $\alpha'\text{-NaV}_2\text{O}_5$ . Two of them fall into the same category, the electric dipole active dynamic DM mech-

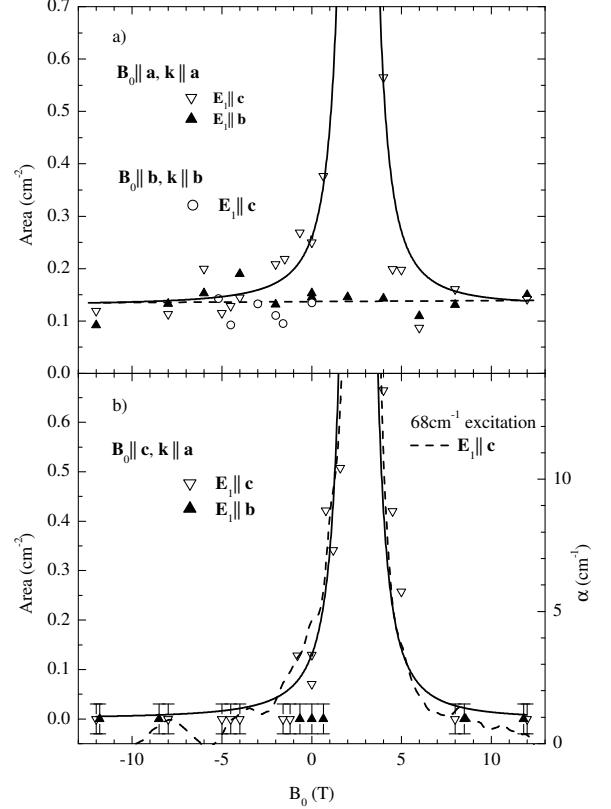


FIG. 14: The magnetic field dependence of the singlet to triplet transition line area at 4.4 K in two polarizations,  $\mathbf{E}_1 \parallel \mathbf{c}$  (empty symbols) and  $\mathbf{E}_1 \parallel \mathbf{b}$  (filled triangles). The line areas are plotted in the negative field direction for the transition to the  $m_S = -1$  triplet level and for the transition to  $m_S = 1$  in the positive field direction. The zero field data points on the graph are one half of the measured area. (a):  $\mathbf{B}_0 \parallel \mathbf{a}$  and  $\mathbf{B}_0 \parallel \mathbf{b}$ . (b):  $\mathbf{B}_0 \parallel \mathbf{c}$ . The dashed line in (a) is a guide for the eye. The dashed line in (b), units on the right axis, is the  $68 \text{ cm}^{-1}$  absorption line shape with the background subtracted and the energy units converted into magnetic field units using the triplet state g-factor,  $g_c = 1.90$ . The error bars shown only in (b) apply to data points in both panels. A solid line in (b) is a fit to the dynamic DM mechanism induced by the  $68 \text{ cm}^{-1}$  phonon. The oscillator strength of the phonon and the singlet to triplet transition in zero field are  $400 \text{ cm}^{-2}$  and  $0.13 \text{ cm}^{-2}$ , respectively. The only fit parameter is the dynamic DM interaction,  $qD_Q = 0.13 \text{ cm}^{-1}$ .

anism. The third contribution is probably due to the static DM interaction mechanism where magnetic dipole transitions are active, but cannot be explained with a single dimer model.

We rule out a possible singlet to triplet absorption mechanism based on a staggered g-factor. The staggered g-factor mechanism requires that the principal axes of the g-tensors of a pair of spins with anisotropic g-factors must not coincide. Let us consider for an example the spin  $\mathbf{S}_1$  with its principal axes rotated from the crys-

tal a-axis by an angle  $\theta$  and the spin  $\mathbf{S}_2$  by an angle  $-\theta$  and  $\mathbf{B}_0 \parallel \mathbf{a}$ . Let the hamiltonian contain isotropic exchange interaction  $J\mathbf{S}_1 \cdot \mathbf{S}_2$  and Zeeman interaction  $\mathbf{B}_0 \cdot (\mathbf{g}_1 \cdot \mathbf{S}_1 + \mathbf{g}_2 \cdot \mathbf{S}_2)$ . Matrix elements between the singlet and triplet states equal to  $\pm B_0(g_a - g_b) \sin \theta \cos \theta$  appear. It is important that the singlet-triplet mixing is proportional to  $B_0$ . *First*, there is no mixing in zero field ( $B_0 = 0$ ) and the staggered g-factor mechanism is turned off. *Second*, the transition probabilities increase as  $(B_0)^2$  if the magnetic field is small compared to the separation of the singlet and triplet states. In the experiment we observe a singlet to triplet transition in zero field, and also the observed magnetic field dependence is different from that of the staggered g-factor mechanism. Therefore this mechanism does not apply to the singlet-triplet transitions in  $\alpha'$ - $\text{NaV}_2\text{O}_5$ .

### 1. Dynamic Dzyaloshinskii - Moriya: $\mathbf{E}_1 \parallel \mathbf{a}$

The strongest singlet to triplet absorption is observed in  $\mathbf{E}_1 \parallel \mathbf{a}$  polarization. There is no resonant enhancement in the magnetic field dependence of the line area as seen in Fig. 12 and any of the optically active excitations in  $\mathbf{E}_1 \parallel \mathbf{a}$  polarization is a candidate that can create the dynamic DM interaction. Nevertheless we can make some choices. The  $91 \text{ cm}^{-1}$  a-axis phonon is not active since no enhancement is observed when the upper branch of the triplet resonance crosses the phonon frequency at 28 T (Fig. 12) although there is an interaction between this phonon and the continuum of magnetic excitations as is manifested by the Fano line shape of the phonon line above  $T_c$  (Fig. 5).

In Fig. 12 we have plotted two fit curves based on perturbation calculation results (Eq-s 13, 14). In one case the phonon frequency was fixed to  $518 \text{ cm}^{-1}$  that is the strongest a-axis optical phonon<sup>31</sup>. In the other case the phonon frequency was a fitting parameter giving us  $(180 \pm 10) \text{ cm}^{-1}$ . This value represents the lowest boundary for the frequency of the DM phonon. Phonons with lower frequencies would give a too steep magnetic field dependence of the singlet to triplet transition probability. It is likely that the lowest boundary of the phonon frequency has been underestimated since the three high field data points above 30 T influence the fit by lowering the phonon frequency. Additional measurements above 33 T are required to clarify this intensity enhancement. Based on these fits the strength of the dynamic DM interaction  $qD_Q$  can be obtained. The closest low  $T$  phase infrared active a-axis phonon in frequency to  $180 \text{ cm}^{-1}$  is the  $199 \text{ cm}^{-1}$  zone folded phonon<sup>31</sup>. The plasma frequencies  $\Omega_p$  of the  $199 \text{ cm}^{-1}$  and  $518 \text{ cm}^{-1}$  phonons are  $48 \text{ cm}^{-1}$  (Ref.<sup>32</sup>) and  $853 \text{ cm}^{-1}$  (Ref.<sup>33</sup>), respectively. We convert the plasma frequency into the line area in absorbance units,  $\int \alpha(\omega) d\omega$ , using  $\int \alpha(\omega) d\omega = \pi^2 \Omega_p^2 / n_a$ . From the fit results we calculate  $qD_Q = 5 \text{ cm}^{-1}$  for the  $199 \text{ cm}^{-1}$  phonon and  $qD_Q = 0.9 \text{ cm}^{-1}$  for the  $518 \text{ cm}^{-1}$  phonon.

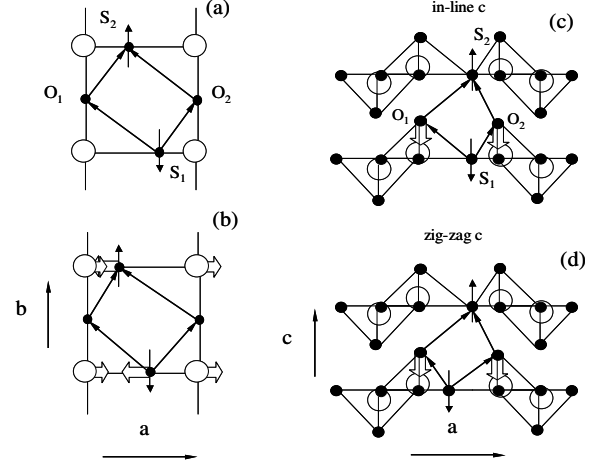


FIG. 15: Cartoons of superexchange paths in the ab-plane (panels (a) and (b)) with one ladder shown and in the ac-plane ((c) and (d)) with two ladders shown. For illustrative purposes it is assumed that the spin is located on the rung oxygen. Oxygens are shown by filled circles and vanadium atoms by open circles. Block arrows show the displacement of atoms due to a phonon. (a) superexchange paths between two spins over on-leg oxygens within the same ladder in the zig-zag ordered phase; (b) same superexchange paths when an a-axis phonon is involved; (c) superexchange paths between two spins in the neighboring planes over apical oxygens displaced by a c-axis phonon when spins are in-line along c-axis or (d) zig-zag.

The orientation of the DM vector is determined by the vector product of the vectors connecting two spins over the superexchange path<sup>34,35</sup>

$$\frac{\mathbf{D}}{|\mathbf{D}|} = [\mathbf{R}_{S_1, O_i} \times \mathbf{R}_{O_i, S_2}] \quad (16)$$

In the zigzag ordered low  $T$  phase two superexchange paths exist, one over on-leg oxygen  $O_1$  and the other over  $O_2$ , shown in Fig. 15(a). The resultant DM vector is zero since the two DM vectors, pointing in  $\mathbf{c}$ -direction, cancel each other. The zero length of the DM vector follows from the general arguments of symmetry too as in this particular case there exists a local center of inversion located between two V-O-V rungs. The  $518 \text{ cm}^{-1}$  a-axis phonon displaces on-rung oxygens along the rung (on-rung V-O-V stretching mode)<sup>36</sup>, Fig. 15(b). Because of the phonon the two superexchange paths are not “equal” any more and the resulting DM vector points along the c-axis. The orientation of the dynamic DM vector,  $\mathbf{D}_Q \parallel \mathbf{c}$ , is consistent with the selection rules for the dynamic DM interaction observed experimentally. The transition to the  $|t_0\rangle$  is observed when  $\mathbf{B}_0 \parallel \mathbf{D}_Q$ , Fig. 11(d). The transitions to the  $|t_{-0}\rangle$  and  $|t_{+0}\rangle$  states are observed when  $\mathbf{B}_0 \perp \mathbf{D}_Q$ , Fig. 11(a), (b), (c).

There is another phonon with an oscillator strength larger than that of the  $518 \text{ cm}^{-1}$  a-axis phonon. That

is the  $582\text{ cm}^{-1}$  b-axis phonon that stretches on-leg V-O-V bonds<sup>31,33</sup>. In the high T phase where electron charge (and spin) is rung-centered, such distortion does not produce any DM interaction from the principles of symmetry. In the low T phase the charges are ordered in a zigzag pattern. The on-leg V-O-V bond stretching phonon lowers the symmetry and creates the DM interaction along the c-axis. We do not observe a singlet to triplet absorption with an electric dipole moment along the b-axis in the experiment. There are two possibilities why the  $\mathbf{E}_1 \parallel \mathbf{b}$  absorption is not observed. *First*, there is no zigzag charge order. *Second*, there is a zigzag charge order and although the dynamic DM is allowed by symmetry, the actual value of  $qD_Q$  is small and the absorption cannot be observed in our experiment. Since there is a mounting evidence in the favor of a low T zigzag charge order<sup>7,8,11</sup> we consider the second case likely.

## 2. Dynamic Dzyaloshinskii - Moriya: $\mathbf{E}_1 \parallel \mathbf{c}$

The singlet to triplet absorption with the electric dipole moment along the c-axis is due to the dynamic DM interaction. In this particular case the dynamic DM mechanism is brought in by the  $68\text{ cm}^{-1}$  optically active c-axis phonon. The enhancement of the singlet-triplet absorption close to the  $68\text{ cm}^{-1}$  line is present if the magnetic field is either parallel to a- or b-axis, but missing if the field is along the c-axis. In Section V C we present further arguments supporting the assignment of the  $68\text{ cm}^{-1}$  resonance to a phonon and not to a magnetic excitation.

In Fig. 14 the fit of the singlet to triplet transition intensities to the dynamic DM absorption mechanism is shown. The input parameters are the resonance frequency of the phonon,  $\omega_p = 68\text{ cm}^{-1}$ , and the frequency of the singlet to triplet transition as the function of magnetic field,  $\omega_{T\pm} = \Delta \pm g\mu_B B_0$ , where  $\Delta = 65.4\text{ cm}^{-1}$ . We estimated the low temperature oscillator strength of the phonon from the  $T$  dependence presented in Fig. 10 and got  $\Omega_p^2 = 400\text{ cm}^{-2}$ . The ratio of the singlet to triplet absorption oscillator strength  $\Omega_{ST}^2$  to the oscillator strength of the phonon,  $\Omega_p^2$ , is  $\Omega_{ST}^2/\Omega_p^2 \sim 0.13/400 = 3.3 \times 10^{-4}$ . The only fit parameter is the strength of the dynamic DM interaction,  $qD_Q = 0.13\text{ cm}^{-1}$ .

We used  $\mathbf{D}_Q \parallel \mathbf{b}$  in our fit because the splitting of the triplet in the magnetic field is observed if  $\mathbf{B}_0 \parallel \mathbf{a}$  or  $\mathbf{B}_0 \parallel \mathbf{c}$  (Fig. 14). According to the selection rules for the dynamic DM only the transitions to the triplet states with  $m_S = 1$  and  $m_S = -1$  are observed when the magnetic field is perpendicular to the dynamic DM vector  $\mathbf{D}_Q \perp \mathbf{B}_0$ . The selection rules for the dynamic DM if  $\mathbf{B}_0 \parallel \mathbf{D}_Q \parallel \mathbf{b}$  allow only transitions to the  $m_S = 0$  level that does not shift with the magnetic field and we do not see it in the differential absorption spectra that are taken in different magnetic fields. The background intensities that do not depend on the magnetic field in figure 14(a) are analyzed in the next section (V A 3).

Which lattice deformations along the c-axis (electric

dipole!) will give the dynamic DM interaction in the b-axis direction? It turns out that we have to consider inter-plane interactions. For the beginning let us consider two spins on the neighboring rungs, as shown in Fig. 15(a), where optical c-axis phonons have the out of (ab) plane anti phase movements of oxygen and vanadium atoms. In the low  $T$  zigzag ordered phase the dynamic DM vector will have components along both, a- and b-axis. The b-axis component of the dynamic DM turns to zero for a vanishing zigzag order, i.e. in the limit of rung-centered spin distribution. The a-axis component stays nonzero. To get a dynamic DM exclusively along the b-axis we have to consider interactions between the spins in the neighboring planes. Here the path for the DM interaction between spins in the neighboring planes goes over the apical oxygens. Two arrangements along the c-axis are possible in the zigzag ordered phase, shown in Fig. 15(c),(d): in-line or zigzag. In both arrangements the displacement of the apical oxygens in the c-direction will create a dynamic DM along the b-axis. As one can see not only the dynamic, but also the static DM in the b-direction is allowed by the symmetry.

In the experiment we do not see magnetic dipole active optical transitions caused by the static DM interaction. To compare the strength of magnetic and electric dipole transitions we must know the magnitude of the static DM interaction. The magnitude of the DM interaction was estimated by Moriya<sup>21</sup>,  $D \approx (|g - g_e|/g_e)J$ , where  $J$  is isotropic exchange interaction and  $g_e = 2$  is the free electron g-factor. We use  $g = 1.90$  and  $J = 60\text{ meV}$  (from Ref.<sup>14</sup>) and get  $D = 25\text{ cm}^{-1}$ . The transition intensity  $I$  is proportional to  $(|V|/\delta\mathcal{E})^2$  where  $|V|$  is the matrix element of the interaction ( $D$  or  $qD_Q$ ) between the two states and  $\delta\mathcal{E}$  is their energy separation. For the static DM effect  $\delta\mathcal{E}$  is the singlet-triplet gap,  $\delta\mathcal{E} = 65.4\text{ cm}^{-1}$ ; for the dynamic DM it is the energy difference between the phonon energy and the triplet level,  $\delta\mathcal{E} = 68 - 65.4 = 2.6\text{ cm}^{-1}$ . The intensity of the magnetic dipole transition is weaker than the electric dipole transition by the factor of  $\alpha_f^{-2} = 137^2$ , where  $\alpha_f$  is the fine structure constant (see Ref.<sup>37</sup> p.171). If we use  $D = 25\text{ cm}^{-1}$  and  $qD_Q = 0.13\text{ cm}^{-1}$  we get that the intensity due to the dynamic mechanism is  $(0.13 \times 65.4)^2 / (\alpha_f 25 \times 2.6)^2 \approx 300$  times larger than the intensity due to the static mechanism. Optical transitions due to the static DM interaction are suppressed with respect to the transitions caused by the dynamic DM because electric dipole transitions are stronger than magnetic dipole transitions.

Our conclusion is that the dynamic DM interaction along the b-axis,  $qD_Q = 0.13\text{ cm}^{-1}$ , is between the spins on the ladders of the neighboring planes. The  $68\text{ cm}^{-1}$  c-axis phonon that creates the dynamic DM interaction involves the displacement of apical oxygens.

### 3. Third optical singlet-triplet absorption mechanism

There is a third mechanism for the optical triplet absorption that is responsible for the magnetic field independent intensities of the transitions to the  $m_S = -1$  and  $m_S = 1$  triplet levels, shown in Fig. 14(a) by solid triangles and empty circles. The same mechanism contributes together with the enhanced part discussed in the previous section to the intensity plotted with empty triangles on the same graph.

We could assume that the third mechanism is also an electric dipole absorption mechanism as the two mechanisms ascribed to the singlet-triplet absorption in  $\mathbf{E}_1 \parallel \mathbf{a}$  and  $\mathbf{E}_1 \parallel \mathbf{c}$  polarizations. Since this absorption is present in both polarizations,  $\mathbf{E}_1 \parallel \mathbf{b}$  and  $\mathbf{E}_1 \parallel \mathbf{c}$  one has to assume that the electric dipole moment is either in the (bc)-plane or, just by coincidence, two electric dipole mechanisms, one polarized along the b-axis and the other polarized along the c-axis, give the same intensities. The case that the optical phonon responsible for the dynamic DM effect has a dipole moment in the (bc)-plane contradicts with the data available on phonons and with the crystal symmetry. The second case of coinciding intensities is ruled out by the selection rules if applied to the full data set presented in Fig. 14(a) and (b).

The third mechanism could be a magnetic dipole DM mechanism. By applying the selection rules to the data we should be able to determine the orientation of the DM vector. According to the theory (section II A) transitions to the  $m_S = -1$  and  $m_S = 1$  states have constant and equal intensities when  $\mathbf{B}_0 \parallel \mathbf{D}$ . This condition is satisfied by two data sets, solid triangles ( $\mathbf{H}_1 \parallel \mathbf{c}$ ) and empty triangles ( $\mathbf{H}_1 \parallel \mathbf{b}$ ) in Fig. 14(a), measured with  $\mathbf{B}_0 \parallel \mathbf{a}$ . We have  $\mathbf{D} \parallel \mathbf{a}$ , where  $I_x^\pm = I_y^\pm$  and  $x \equiv b$  and  $y \equiv c$  (see Fig. 1). However the set represented by the circles in Fig. 14(a) is the  $I_y^\pm$  intensity in the perpendicular configuration,  $\mathbf{B}_0 \perp \mathbf{D}$  (in our notation  $\mathbf{D} \parallel \mathbf{y} \parallel \mathbf{a}$ ), which should have zero intensity according to the theory (see Fig. 2). Also, in the  $\mathbf{B}_0 \parallel \mathbf{H}_1 \parallel \mathbf{c}$  configuration  $I_z^\pm$  should have non-zero intensities. In the experiment, filled triangles in Fig. 14(b), no intensity is observed contrary to the theory. Therefore the assumption  $\mathbf{D} \parallel \mathbf{a}$  is not consistent with the full data set. Also, we can prove that neither  $\mathbf{D} \parallel \mathbf{b}$  nor  $\mathbf{D} \parallel \mathbf{c}$  is fully consistent with the experiment.

Our conclusion is that the third optical triplet absorption mechanism is a magnetic dipole transition, but cannot be explained by an isolated dimer model with DM interactions. Apparently, a more elaborate model including the inter-dimer DM interactions, is necessary.

### B. Spin gap and phase transition

We studied the effect of temperature and magnetic field on the singlet to triplet transition. The results are shown with circles in Fig. 8. We observe that the intensity of the singlet to triplet transition (Fig. 8(a)) follows the intensity of the X-ray diffraction peak<sup>38</sup> reported in the same

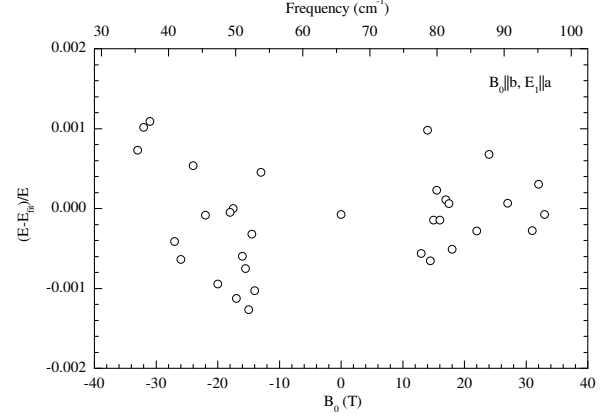


FIG. 16: Relative deviation  $(E - E_{fit})/E$  of S to  $T_{-1}$  (plotted at negative field values) and S to  $T_{+1}$  (plotted at positive field values) transition energy  $E$  from the linear fit  $E_{fit}$ .

figure. Gaulin *et al.* have shown that the intensity of the X-ray diffraction peak can be fitted with a single function  $I = t^\beta$  over the reduced temperature,  $t = 1 - T/T_c$ , in the range from  $6 \times 10^{-3}$  to  $2 \times 10^{-2}$  with the critical exponent  $\beta = 0.18$ . Our data taken below 30 K is above  $1.1 \times 10^{-1}$  in the reduced temperature scale, which is unsuitable for the determination of the critical exponent.

The singlet-triplet splitting (spin gap), shown in Fig. 8(b), is more rigid than the singlet to triplet transition probability or the X-ray scattering intensity. The rigidity of the spin gap has been confirmed earlier by INS measurements<sup>3</sup> and by high field electron spin resonance measurements, although not in the zero magnetic field<sup>16</sup>. The far-infrared S to T gap is in agreement with the INS gap also shown in Fig. 8(b). In the ultrasonic experiment<sup>39</sup> the measurements were extended close enough to  $T_c$  that one is able to determine the critical exponent for the spin gap. The temperature dependence of the spin gap, measured indirectly by the ultrasonic probe, gives the critical exponent  $\beta = 0.34$  below the reduced temperature  $10^{-2}$ . Although far-infrared measurements of the gap are direct, reasonable data can be obtained only too far from  $T_c$  as the absorption line broadens and gets weak and therefore the fit, inset to Fig. 8(b), gives us an exceptionally low critical exponent,  $\beta = 0.039 \pm 0.002$ .

The magnetic field dependence of the spin gap and the triplet state g-factor have been measured up to 33 T for one field orientation,  $\mathbf{B}_0 \parallel \mathbf{b}$ , at 4.7 K. The line positions of the transitions from the singlet ground state to the triplet states with  $m_S = \pm 1$  were fitted with a linear function  $E_{fit} = \Delta \pm g\mu_B B_0$ . The reduced residual of the linear fit is less than 0.0012 of the transition energy, as shown in Fig. 16. This means that the triplet state g-factor is not renormalized by the magnetic field as high as 33 T and the spin gap is independent of the field up to 33 T. The independence of the gap value  $\Delta$  on the field at

low temperature is not surprising<sup>40</sup>. The role of the magnetic field is to couple to thermally excited quasiparticles. At low temperature the number of quasiparticles is small and hence the effect of the magnetic field is negligible.

In conclusion, the temperature dependence of the intensity of the singlet to triplet transition agrees with the X-ray scattering intensity temperature dependence. Also, the singlet-triplet splitting at 8.13 meV has the same temperature dependence as the singlet-triplet splitting of the second excitation branch at 9.8 meV measured by the INS. The 8.13 meV spin gap is not altered by the magnetic field at least up to 33 T.

### C. Phonons and phase transition

#### 1. *c*-axis phonons

In Section V A 2 while calculating the dynamic DM interaction for  $\mathbf{E}_1 \parallel \mathbf{c}$  we assumed that the electric dipole moment of the *c*-axis polarized optical singlet to triplet transition comes from the interaction between the spin system and the  $68 \text{ cm}^{-1}$  optical *c*-axis phonon. An alternative would be that the  $68 \text{ cm}^{-1}$  resonance is not a phonon but a singlet electronic excitation. Here we analyze existing data and show that the data is not in contradiction with the assumption that the  $68 \text{ cm}^{-1}$  resonance is a phonon mode.

There is a series of infrared-active *c*-axis modes appearing below 34 K as shown in Fig. 6 and found by other groups<sup>32,41</sup>. The two low frequency modes, at  $68$  and  $106 \text{ cm}^{-1}$ , are the strongest. The temperature dependence of their resonance frequencies plotted in Fig. 17(a) is an order of magnitude larger as compared to the *a*- and *b*-polarized modes plotted in Fig. 17(b). Modes at frequencies close to  $68$  and  $106 \text{ cm}^{-1}$  have been found by Raman spectroscopy<sup>42,43</sup>. Sample dependence of mode frequencies by few wavenumbers has been observed both in infrared<sup>32</sup> and Raman<sup>43</sup>. It is known that Na deficiency of  $\alpha'\text{-Na}_x\text{V}_2\text{O}_5$  affects  $T_c$  and in samples where  $x = 0.97$  the phase transition is suppressed completely<sup>44</sup>. A Na doping dependence study<sup>43</sup> has shown that the frequency variation of Raman modes from sample to sample is related to the Na content of the sample. Raman measurements<sup>45</sup> on the sample from the same batch as the one studied here gave values for the mode frequencies  $65.9$  and  $105 \text{ cm}^{-1}$  at  $4.4 \text{ K}$ . This means that Raman and infrared spectroscopy observe different modes since the frequencies of infrared modes are  $68$  and  $106 \text{ cm}^{-1}$ . Neither of the Raman modes<sup>42,43</sup> nor the infrared modes (this work and Ref.<sup>41</sup>) split in the magnetic field. The comparison of the  $T$  dependence of the normalized mode frequency has shown that the  $T$  dependence of the  $65.9 \text{ cm}^{-1}$  Raman mode follows the  $T$  dependence of the  $68 \text{ cm}^{-1}$  infrared mode and the  $105 \text{ cm}^{-1}$  Raman mode follows the  $T$  dependence of the  $106 \text{ cm}^{-1}$  infrared mode. Therefore, although the infrared and the Raman modes do not have the same frequencies, it is likely that the

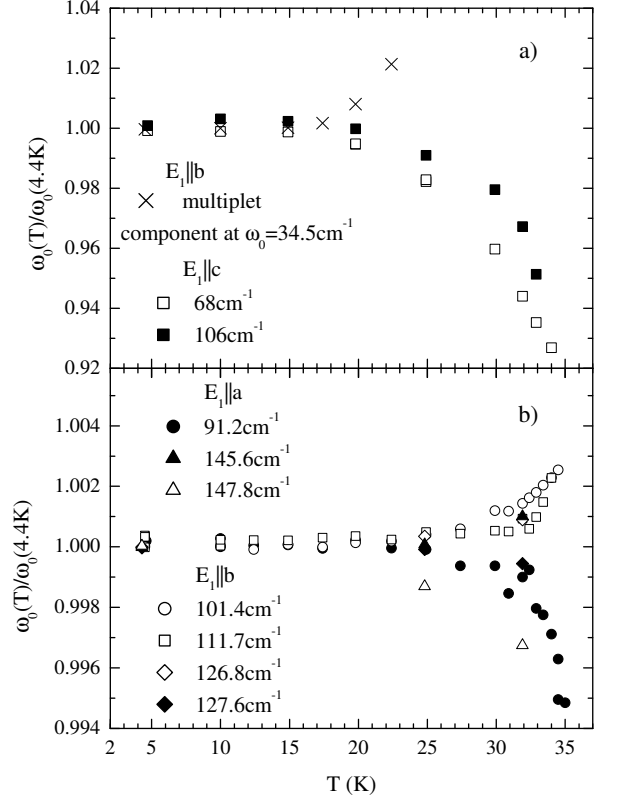


FIG. 17: Temperature dependence of normalized phonon frequencies. (a) - *b*-axis multiplet and *c*-axis phonons, (b) - *a*- and *b*-axis phonons.

origin of the infrared and Raman modes near  $68$  and  $106 \text{ cm}^{-1}$  is the same, lattice modes or electronic excitations.

The origin of the low frequency infrared and Raman modes has been under the debate. It has been concluded that the Raman modes are not lattice vibrations<sup>42,43</sup>. In Ref.<sup>32</sup> the conclusion was that the infrared modes at  $68$  and  $106 \text{ cm}^{-1}$  are zone-folded *c*-axis phonons and it was speculated that their peculiar  $T$  dependence compared to other zone-folded phonon modes is caused by the interaction of phonons with charge and spin degrees of freedom. Indeed, the  $68 \text{ cm}^{-1}$  mode and the singlet to triplet excitation at  $65.4 \text{ cm}^{-1}$  have similar  $T$  dependencies of their infrared absorption line parameters as shown in Fig. 8. Assuming that  $68$  and  $106 \text{ cm}^{-1}$  excitations are zone folded phonons we would have to explain why their frequencies depend on Na deficiency and why their frequencies have a different temperature dependence than the other zone-folded modes have. We argue that both points can be explained if charge correlations develop inside ladder planes prior to the transition to the low  $T$  phase and at the phase transition three-dimensional correlations build up between the planes.

Charge ordering within ladder planes precedes the lat-

tice distortion and the opening of the spin gap as evidenced by the vanadium Knight shift and the sodium quadrupolar and Knight shifts<sup>10</sup>. The presence of two-dimensional charge correlations in the ladder planes above 35 K is also supported by the X-ray diffraction measurements<sup>38</sup>. In  $\alpha'$ - $\text{NaV}_2\text{O}_5$  there are modulated ladders with a zigzag charge order within one plane<sup>7,9,10</sup>. It is possible to construct four different planes with the zigzag charge order and when stacked in certain sequence along the c-axis a unit cell is formed compatible with the observed X-ray structure<sup>8,11</sup>. By applying pressure the critical temperature is reduced and it has been found that the soft axis is the c-axis<sup>27,46</sup>. A “devil’s staircase” like sequence of phase transitions to the phases with unit cells incorporating more than four planes in the c-direction takes place under pressure larger than 0.5 GPa<sup>47</sup>. Therefore the interactions between layers are important in the formation of three dimensional correlations.

Interactions between ladder planes are important for those modes, which are zone-folded along the c-axis. The primary candidates are the modes with anti-phase movements of atoms along the c-axis in the neighboring planes, which are naturally the modes that are polarized along the c-axis. The c-axis modes have the largest frequency shift close to the phase transition point. The exception is the b-polarized multiplet (Fig. 9). It is the only non-c-axis low frequency mode, which has a relative change of frequency with temperature (Fig. 17(a)) that is comparable to the c-axis modes. Considering the low frequency of the multiplet it is likely that the seven lines are a result of the folding of a b-polarized acoustical, not optical phonon branch. To get seven optical phonon branches out of one phonon branch a c-axis folding is required in addition to a- and b-axis foldings. Therefore this multiplet involves relative movements of atoms in neighboring layers and is a subject to interlayer couplings.

Our conclusion is that the c-axis phonon modes are most susceptible to three dimensional correlations between ladder planes and therefore their  $T$  dependence is different from other low frequency phonon modes. We assign the  $68\text{ cm}^{-1}$  (and  $106\text{ cm}^{-1}$ ) infrared active mode and the  $66\text{ cm}^{-1}$  (and  $105\text{ cm}^{-1}$ ) Raman active modes to the zone-folded phonons.

## 2. Polarization dependence of line intensities

In  $\text{NaV}_2\text{O}_5$  the a- and b-axes are not equivalent and one would expect the selection rules to apply so that the phonon active in the  $\mathbf{E}_1 \parallel \mathbf{a}$  absorption is missing in  $\mathbf{E}_1 \parallel \mathbf{b}$  spectrum and vice versa. In other words, phonons polarized along a-axis should have different frequencies than phonons polarized along the b-axis.

This rule applies well at 40 K (Fig. 5). The strong  $180\text{ cm}^{-1}$  phonon is missing in the  $\mathbf{E}_1 \parallel \mathbf{a}$  spectrum and the structure at  $140\text{ cm}^{-1}$  is missing in the  $\mathbf{E}_1 \parallel \mathbf{b}$  spectrum. The  $90.7\text{ cm}^{-1}$  line is present only in the  $\mathbf{E}_1 \parallel \mathbf{a}$  spectrum.

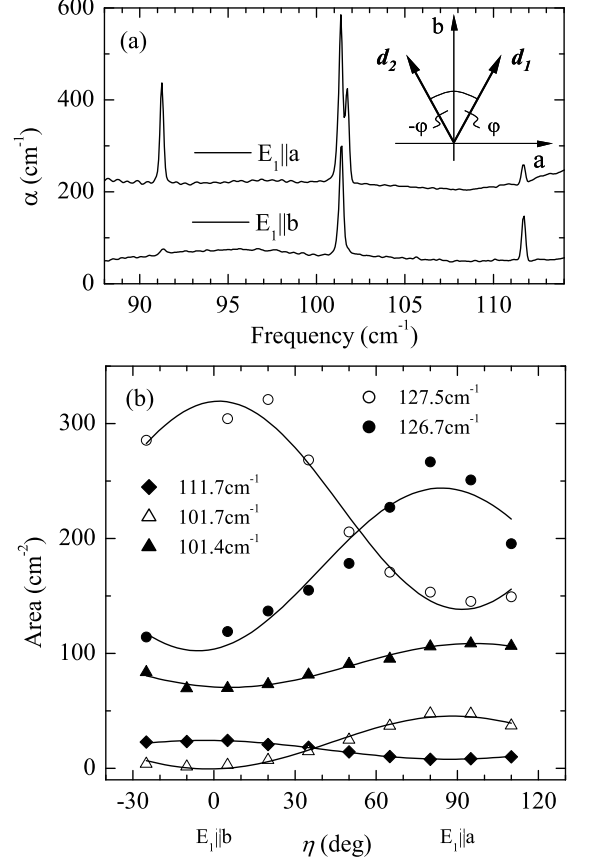


FIG. 18: Polarization dependence of low frequency phonon absorption line intensities. (a) - absorption spectra in  $\mathbf{E}_1 \parallel \mathbf{a}$  (shifted upwards by  $150\text{ cm}^{-1}$ ) and  $\mathbf{E}_1 \parallel \mathbf{b}$  polarizations. (b) - absorption line areas as a function of polarization angle in the (ab)-plane;  $\eta = 0$  corresponds to  $\mathbf{E}_1 \parallel \mathbf{b}$ . Inset to (a) shows the orientation of electric dipoles rotated from the b-axis by an angle  $\varphi$  and  $-\varphi$ .

At 4.4 K this selection rule does not apply to all absorption lines. The  $101.4$  and  $111.7$ ,  $126.7$  and  $127.5\text{ cm}^{-1}$  phonons (Fig.-s 18(a), 5) have absorption in both polarizations. The leakage of the wrong polarization through the polarizer is ruled out. For example, the  $101.7\text{ cm}^{-1}$  line present in  $\mathbf{E}_1 \parallel \mathbf{a}$  spectrum is missing in  $\mathbf{E}_1 \parallel \mathbf{b}$  spectrum (Fig. 18a) and the multiplet at  $30\text{ cm}^{-1}$  is missing in  $\mathbf{E}_1 \parallel \mathbf{a}$  spectrum (Fig. 5).

We measured the polarization dependence of line in-

TABLE II: Rotation angle  $\varphi$  calculated from the two dipole model.  $\varphi_a$  ( $\varphi_b$ ) is the rotation angle of the phonon dipole moment from the crystal a-axis (b-axis).

$\omega_0$ ( $\text{cm}^{-1}$ )	101.4	101.7	111.7	126.8	127.5
$\varphi_b \equiv \varphi$	—	—	32	—	35
$\varphi_a = 90^\circ - \varphi$	37	0	—	31	—



tensities in the (ab)-plane. The areas of absorption lines between 100 and 130 cm<sup>-1</sup> are plotted in Fig. 18(b) as a function of the angle  $\eta$  between the polarizer and the b-axis. The lines at 91 cm<sup>-1</sup> were not included since they are two different lines, one at 91.2 cm<sup>-1</sup> in the a-polarization and the other at 91.3 cm<sup>-1</sup> in the b-polarization. As the 101.7 cm<sup>-1</sup> line has zero intensity at  $\eta = 0^\circ$ ,  $\mathbf{E}_1 \parallel \mathbf{b}$  it belongs to the phonon modes representing the averaged crystal symmetry. It is important that the intensity of the 101.4 cm<sup>-1</sup>, 111.7 cm<sup>-1</sup>, 126.7 cm<sup>-1</sup> and 127.5 cm<sup>-1</sup> lines never falls to zero between  $\eta = 0^\circ$  and  $90^\circ$ . A similar effect was found by Damascelli *et al.*<sup>31</sup> for several infrared active phonons at higher frequencies. The simplest explanation would be that the zone-folded a- and b-polarized phonons are pair wise degenerate, but then it is hard to explain why there is a constant intensity ratio of at least four pairs of low frequency and of one high frequency (718 cm<sup>-1</sup>) pair of a- and b-axis phonons, as is shown below.

We assume, as was done in Ref.<sup>31</sup>, that there are two regions in the crystal with a symmetry different from the averaged crystal symmetry. In one region the electric dipole moment of a phonon,  $\mathbf{d}$ , is rotated from the crystal b-axis by an angle  $\varphi$  and in the other region by  $-\varphi$  as shown in the inset to Fig. 18(a). The optical conductivity in the first region is  $\sigma_1(\varphi) = aE_1^2 d^2 \cos^2(\varphi - \eta)$ , where  $a$  is a constant independent of angular parameters.  $\eta$  is the angle between the b-axis and the electric field vector of light  $\mathbf{E}_1$ . The conductivity in the second region is  $\sigma_1(-\varphi) = aE_1^2 d^2 \cos^2(\varphi + \eta)$ . Since the phonons are independent in the two regions the total observed conductivity is  $\sigma_1 = \sigma_1(\varphi) + \sigma_1(-\varphi) = I_b \cos^2 \eta + I_a \sin^2 \eta$ , where  $I_b = 2aE_1^2 d^2 \cos^2 \varphi$  and  $I_a = 2aE_1^2 d^2 \sin^2 \varphi$  are the oscillator strengths observed in the experiment in the b- and a-polarizations respectively. The solid lines in Fig. 18(b) are the fits of the integrated absorption line areas where Eq. 15 has been used to convert  $\alpha(\omega)$  into  $\sigma_1(\omega)$ . The results are given in Table II. Note that two of the absorption lines belong to the dipoles rotated from the a-axis and two to the dipoles rotated by approximately the same angle from the b-axis. The averaged value of the rotation of the dipole moment is  $\bar{\varphi} = 34^\circ \pm 3^\circ$ . A similar result,  $\varphi = 39^\circ$ , we obtain for the 718 cm<sup>-1</sup> phonon using the data from the Ref.<sup>31</sup> where the given oscillator strength in the  $\mathbf{E}_1 \parallel \mathbf{a}$  polarization is 0.021 and in the  $\mathbf{E}_1 \parallel \mathbf{b}$  polarization is 0.014.

The two regions with a symmetry that is different from the crystal symmetry can be associated with two types of ladder planes with a zigzag charge order. In Ref.<sup>31</sup> it was assumed that the crystal is split into domains with two different diagonal charge patterns. Considering the recent X-ray studies<sup>8,11</sup> it is more likely that there are no domains and two types of planes exist with different diagonal charge pattern instead. The two different charge configurations come from the way the two neighboring zigzag charge ordered ladders are positioned with respect to each other within the plane. A shift of every second ladder by one half of the superlattice constant in the b-

direction creates two different structures where charged stripes of  $V^{+4.5-\delta_c/2}$  run diagonal from left to the right or from right to the left in the (ab)-plane<sup>11</sup>. This diagonal charge order within a single ladder plane determines the orientation of the phonon dipole moments. It is possible to estimate the charge offset  $x = l(1 + \delta_c)/2$  from the center of the rung knowing the tilt angle of the dipole moments  $\varphi$ . Here  $l$  is the length of the rung and the charge transfer factor  $\delta_c$  is associated with the formal valence of vanadium ions in the low  $T$  zigzag ordered phase,  $V^{+4.5-\delta_c/2}$  and  $V^{+4.5+\delta_c/2}$ . The charge transfer factor depends only on the angle  $\varphi$ ,  $\delta_c \approx \tan \varphi$ , since the rung length is approximately equal to the distance between the nearest neighbor V atoms along the leg. We get  $\delta_c = 0.67 \pm 0.07$  using  $\varphi = \bar{\varphi}$ . From the analysis of INS data the authors of Ref.<sup>14</sup> come to a similar value,  $\delta_c = 0.6$ .

Our study of phonon modes in the low temperature phase supports the view that the symmetry of the individual ladder planes is lower than the averaged crystal symmetry. In addition it has been found by sound velocity measurements<sup>48</sup> that the  $c_{66}$  shear mode couples to the pre-transitional charge fluctuations of  $B_{1g}$  symmetry, which correspond to the static zigzag charge order in the low  $T$  phase. There are phonon modes in  $\alpha'$ -NaV<sub>2</sub>O<sub>5</sub> in the low  $T$  phase where the normal coordinates are confined into single ladder planes. These modes show the symmetry of an individual plane determined by the zigzag charge ordering. For other modes the movement of atoms is correlated between the neighboring planes or they are insensitive to the zigzag charge order and therefore they reflect the averaged crystal symmetry.

From the analysis of the infrared spectra we conclude that two types of ladder planes exist with the zigzag charge order where the charged stripes are aligned approximately in  $[110]$  or in  $[\bar{1}10]$  directions. The formal charge of the vanadium atoms forming the zigzag pattern is  $+4.17 \pm 0.04$  and  $+4.83 \pm 0.04$ .

#### D. Continuum of excitations and Fano resonances

A broad absorption continuum is observed in  $\mathbf{E}_1 \parallel \mathbf{a}$  polarization above  $T_c$  that starts gradually below 20 cm<sup>-1</sup> (Fig. 5(a)) and extends up to 400 cm<sup>-1</sup> (Ref.<sup>31</sup>). The change of the continuum with temperature is correlated with the phase transition at 34 K as demonstrated in Fig. 19 where normalized optical conductivity is plotted for three different frequencies. The continuum absorption at 4.4 K shows a threshold at 130 cm<sup>-1</sup> in  $\mathbf{E}_1 \parallel \mathbf{a}$  polarization while at lower frequencies it is similar to the absorption in  $\mathbf{E}_1 \parallel \mathbf{b}$  polarization (Fig. 20). It is natural to associate the absorption continuum with an optical excitation of two triplets since the lowest in energy one triplet excitation is at 65.4 cm<sup>-1</sup>.

There are two derivative-like phonon absorption lines, one at 91.2 and the other at 140 cm<sup>-1</sup>, in the  $\mathbf{E}_1 \parallel \mathbf{a}$  absorption spectrum above  $T_c$  in Fig. 5(a). This line shape,

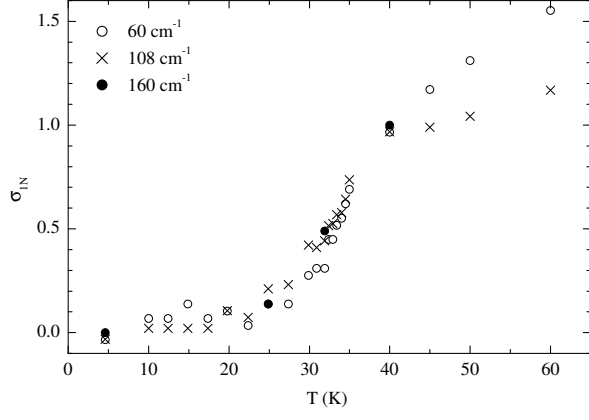


FIG. 19: Temperature dependence of the normalized optical conductivity in  $\mathbf{E}_1 \parallel \mathbf{a}$  polarization  $\sigma_N = [\sigma_{1a}(T) - \sigma_{1a}(4.4K)][\sigma_{1a}(40K) - \sigma_{1a}(4.4K)]^{-1}$  at 60 (open circles), 108 (crosses), and 160  $\text{cm}^{-1}$  (filled circles).

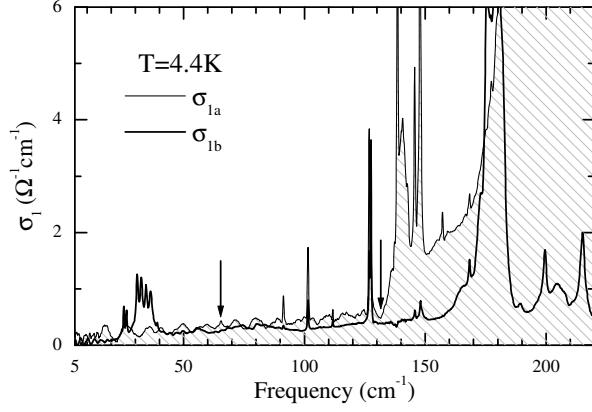


FIG. 20: Real parts of optical conductivities  $\sigma_{1a}$  (shaded and thin line) in  $\mathbf{E}_1 \parallel \mathbf{a}$  polarization and  $\sigma_{1b}$  (thick line,  $\mathbf{E}_1 \parallel \mathbf{b}$ ) at 4.4 K. Arrows point to the singlet to triplet resonance at  $65.4\text{cm}^{-1}$  and to the onset of the absorption continuum at  $132\text{cm}^{-1}$  in  $\mathbf{E}_1 \parallel \mathbf{a}$  polarization.

known as the Fano resonance, comes from the interaction of a discrete level and a continuum of states<sup>49,50</sup>. The Fano lineshape<sup>50</sup> does not describe a normal absorption-like lineshape. To account for an arbitrary line shape, including the lorentzian line, we use an empirical formula<sup>51</sup> for the dielectric function  $\epsilon(\omega)$  where the asymmetry is described by the phase  $\theta$ :

$$\epsilon(\omega) = \epsilon_\infty + \frac{\Omega_p^2 \exp(-i\theta)}{\omega_p^2 - \omega^2 - i\omega\gamma}. \quad (17)$$

$\Omega_p$  is the plasma frequency,  $\epsilon_\infty$  is the background dielectric constant, and  $\omega_p$  is the resonance frequency of the phonon, and  $\gamma$  is the full width at half maximum

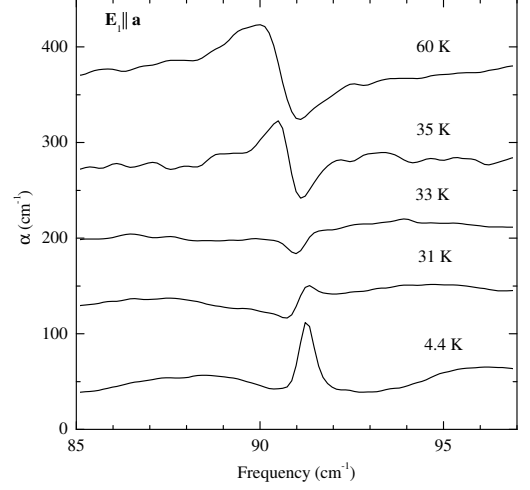


FIG. 21: Temperature dependence of the  $91\text{cm}^{-1}$  phonon absorption line in  $\mathbf{E}_1 \parallel \mathbf{a}$  polarization. Spectra have been off-set by  $50\text{cm}^{-1}$  in vertical direction.

(FWHM) of the lorentzian line at  $\theta = 0$ .

We did a  $T$  dependence study of the  $91\text{cm}^{-1}$  line and the evolution of this line with  $T$  is shown in Fig. 21. The phonon line at  $140\text{cm}^{-1}$  is on a steeply rising background. Since the frequency dependence of the absorption background is not known it is difficult to subtract the background reliably and we did not attempt to evaluate the  $T$  dependence of the  $140\text{cm}^{-1}$  line parameters. The absorption lines were fit with Eq. 17. The relation between the real part of the conductivity and dielectric function is  $\sigma_1(\omega) = \omega \text{Im}[\epsilon(\omega)]/60$ , where  $\sigma_1$  is in units  $\Omega^{-1}\text{cm}^{-1}$  and Eq. 15 was used to calculate  $\sigma_1$  from the measured absorption spectra. The fit parameters are plotted in Fig. 22. The phase  $\theta$  (Fig. 22(d)) changes from  $3\pi/2$  at 35 K to  $\pi$  at 33 K where the line has the shape of an antiresonance (Fig. 21). At 31 K the line has a derivative-like lineshape again, but with a phase  $\pi/2$ . Also the phonon resonance frequency  $\omega_p$  stays fairly constant at higher temperatures and changes abruptly at 35 K. The line area  $S$  and  $\gamma$  have a smooth  $T$  dependence around  $T_c = 35\text{K}$ . At 4.4 K  $\theta = 0$  and the normal lineshape is recovered. The line width  $\gamma$  (Fig. 22(a)) goes down with  $T$  and is limited by the  $0.4\text{cm}^{-1}$  instrumental resolution for this  $T$  dependence study. We know from the higher resolution measurement that the line width is  $0.2\text{cm}^{-1}$  or less at 4.4 K. The line area (Fig. 22(c)) has a different  $T$  dependence than other parameters, having a minimum at approximately 32 K.  $S$  changes substantially even above  $T_c$ , by a factor of 2 from 35 to 40 K.

In this paper we will not present a theory covering the optical conductivity of a system where phonons interact with a two-particle continuum of magnetic excitations. A proper theory must account for a microscopic mechanism responsible for the optical absorption continuum<sup>52</sup>.

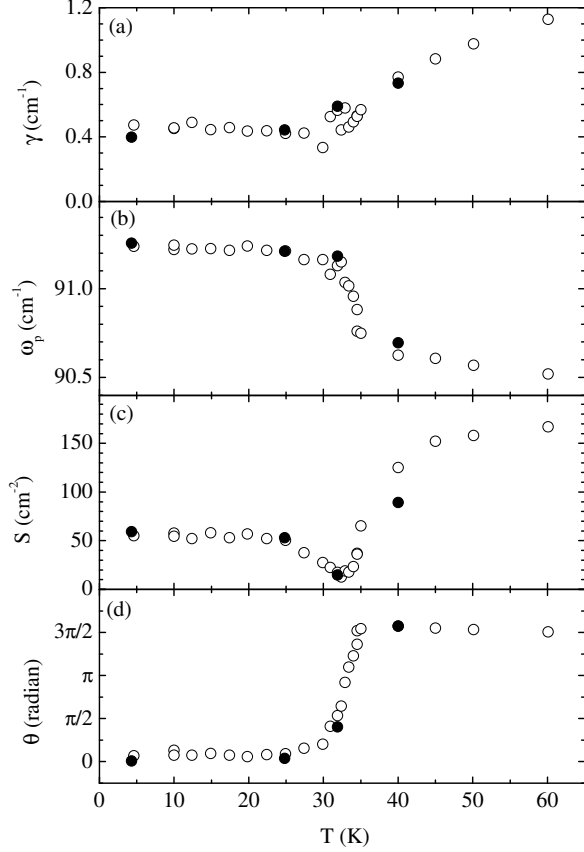


FIG. 22: Temperature dependence of the Fano fit parameters of the  $91\text{ cm}^{-1}$  phonon line: (a) - full width at half maximum  $\gamma$ , (b) - phonon resonance frequency  $\omega_p$ , (c) - integrated line area  $S$ , (d) - asymmetry parameter  $\theta$ . Open circles -  $120\text{ }\mu\text{m}$  thick sample; filled circles -  $40\text{ }\mu\text{m}$  thick sample.

Nevertheless, some observations can be made based on the empirical fit of the phonon line shape. The phase  $\theta$  that is related to the Fano parameter  $q$ ,  $q^{-1} \propto \tan(\theta/2)$ , depends on the strength of the interaction between the phonon and the magnetic system. The  $T$  dependence of  $\theta$  shows that the spin-phonon interaction weakens as  $T$  is lowered below  $35\text{ K}$ . The other reason why the normal lineshape of the  $91\text{ cm}^{-1}$  phonon at low  $T$  is recovered could be vanishing of the two particle absorption continuum below  $130\text{ cm}^{-1}$ . The direct evidence that the spin-phonon interaction is switched off or is very weak at low temperatures is the lorentzian shape of the  $140\text{ cm}^{-1}$  phonon line.

In conclusion, our data shows that there is an absorption continuum in the a-axis polarized optical absorption that develops a gap at low  $T$ . This gap,  $130\text{ cm}^{-1}$ , is equal to twice the singlet-triplet excitation energy,  $65.4\text{ cm}^{-1}$ . Therefore the absorption continuum can be assigned to an absorption of a photon with a simultaneous creation of two magnetic (spin) excitations. Two

low frequency a-axis polarized optical phonons, at  $91$  and  $140\text{ cm}^{-1}$  interact with the magnetic system as evidenced by their derivative-like line shape in the high  $T$  phase.

## VI. CONCLUSIONS

Using far-infrared spectroscopy we have probed spin excitations and phonons in the quarter-filled spin ladder compound  $\alpha'\text{-NaV}_2\text{O}_5$ . The interaction between the spins and the phonons is observed in the gapped spin state below  $34\text{ K}$  and above, in the paramagnetic phase.

The zigzag charge order within the ladders in the gapped state is in accordance with the polarization dependence of several infrared active zone-folded optical phonons. In the high  $T$  phase two a-axis optical phonons interact with the continuum of excitations as manifested by the Fano line-shape of phonon lines. At low  $T$  the continuum absorption is gapped with a threshold energy  $130\text{ cm}^{-1}$ , twice the singlet-triplet gap, and the interaction between the phonons and the continuum of excitations is turned off.

The strength of the singlet to triplet absorption at  $65.4\text{ cm}^{-1}$  is strongly anisotropic. Absorption is strongest when the electric field of the incident light is polarized along the ladder rungs ( $\mathbf{E}_1 \parallel \mathbf{a}$ ). In this polarization the strength of the singlet to triplet absorption has a weak magnetic field dependence up to  $28\text{ T}$ . In  $\mathbf{E}_1 \parallel \mathbf{c}$  polarization a strong magnetic field dependence of the singlet-triplet absorption is observed. This field dependence is due to the dynamic DM interaction created by the  $68\text{ cm}^{-1}$  c-axis optical phonon. In the case of the dynamic DM absorption mechanism the singlet-triplet absorption is electric dipole active and the polarization of the transition is determined by the polarization of the optical phonon creating the dynamic DM interaction by the lattice deformation. Using the presented theory we calculated the strength of the dynamic DM interaction. The dynamic DM interaction,  $qD_Q = 0.13\text{ cm}^{-1}$ , created by the  $68\text{ cm}^{-1}$  c-axis optical phonon is inter-ladder between the spins in the neighboring planes and points along the b-axis. We assign the strong a-axis polarized absorption also to a dynamic DM effect, in this case due to the lattice deformation caused by one of the high frequency a-axis optical phonons. This dynamic DM interaction is intra-ladder and is along the c-axis. Above  $28\text{ T}$  an increase in the S to  $T_+$  a-axis absorption intensity is observed. The origin of the mechanism responsible for that increase is not clear and additional measurements above  $33\text{ T}$  are required.

To summarize, the optical singlet to triplet transition in  $\alpha'\text{-NaV}_2\text{O}_5$  is dominated by an electric dipole active mechanism. We have observed the resonant enhancement of the singlet to triplet transition close to the c-axis  $68\text{ cm}^{-1}$  mode. We described the enhancement of the electric dipole transition with the theory of the dynamic DM mechanism and assigned the  $68\text{ cm}^{-1}$  mode to a c-axis optical phonon. From the analysis of the

phonon infrared spectra we concluded that two types of ladder planes exist with the zigzag charge order along the ladders where the charged stripes across the ladders are aligned approximately in  $[110]$  or in  $[\bar{1}10]$  directions.

## VII. ACKNOWLEDGMENTS

We thank G. Blumberg and O. Cépas for helpful discussions. Work in Tallinn was supported by the Esto-

nian Science Foundation grants 3443, 4926, and 4927. A portion of the work was performed at the National High Magnetic Field Laboratory, which is supported by NSF Cooperative Agreement No. DMR-0084173 and by the State of Florida. U. Nagel was supported by a NATO expert visit grant PST.EV.978692.

We thank a referee of this paper for pointing out that without the Shekhtman correction the DM term lowers the three-fold degeneracy of the triplet state<sup>22,23</sup>.

- 
- \* Electronic address: roomtom@kbfi.ee
- <sup>1</sup> M. Hase, I. Terasaki, and K. Uchinokura, Phys. Rev. Lett. **70**, 3651 (1993).
  - <sup>2</sup> M. Isobe and Y. Ueda, J. Phys. Soc. Jpn. **65**, 1178 (1996).
  - <sup>3</sup> Y. Fujii, H. Nakao, T. Yosihama, M. Nishi, K. Nakajima, K. Kakurai, M. Isobe, Y. Ueda, and H. Sawa, J. Phys. Soc. Jpn. **66**, 326 (1997).
  - <sup>4</sup> W. Schnelle, Y. Grin, and R. K. Kremer, Phys. Rev. B **59**, 73 (1999).
  - <sup>5</sup> S. G. Bompadre, A. F. Hebard, V. N. Kotov, D. Hall, G. Maris, J. Baas, and T. T. M. Palstra, Phys. Rev. B **61**, R13321 (2000).
  - <sup>6</sup> D. C. Johnston, R. K. Kremer, M. Troyer, X. Wang, A. Klümper, S. L. Budko, A. F. Panchula, and P. C. Canfield, Phys. Rev. B **61**, 9558 (2000).
  - <sup>7</sup> H. Nakao, K. Ohwada, N. Takesue, Y. Fujii, M. Isobe, Y. Ueda, M. v. Zimmerman, J. P. Hill, D. Gibbs, J. C. Woicik, et al., Phys. Rev. Lett. **85**, 4349 (2000).
  - <sup>8</sup> S. Grenier, A. Toader, J. E. Lorenzo, Y. Joly, B. Grenier, S. Ravy, L. P. Regnault, H. Renevier, J. Y. Henry, J. Jegoudez, et al., Phys. Rev. B **65**, 180101 (2002).
  - <sup>9</sup> T. Ohama, H. Yasuoka, M. Isobe, and Y. Ueda, Phys. Rev. B **59**, 3299 (1999).
  - <sup>10</sup> Y. Fagot-Revurat, M. Mehring, and R. K. Kremer, Phys. Rev. Lett. **84**, 4176 (2000).
  - <sup>11</sup> S. van Smaalen, P. Daniels, L. Platinus, and R. K. Kremer, Phys. Rev. B **65**, 060101 (2002).
  - <sup>12</sup> K. Ohwada, Y. Fujii, N. Takesue, M. Isobe, Y. Ueda, H. Nakao, Y. Wakabayashi, Y. Murakami, K. Ito, Y. Amemiya, et al., Phys. Rev. Lett. **87**, 086402 (2001).
  - <sup>13</sup> T. Yosihama, M. Nishi, and Y. Ueda, J. Phys. Soc. Jpn. **67**, 744 (1998).
  - <sup>14</sup> B. Grenier, O. Cépas, L. P. Regnault, J. E. Lorenzo, T. Ziman, J. P. Boucher, A. Hiess, T. Chatterji, J. Jegoudez, and A. Revcolevschi, Phys. Rev. Lett. **86**, 5966 (2001).
  - <sup>15</sup> S. Luther, H. Nojiri, M. Motokawa, M. Isobe, and Y. Ueda, J. Phys. Soc. Jpn. **67**, 3715 (1998).
  - <sup>16</sup> H. Nojiri, S. Luther, and Y. Ueda, J. Phys. Soc. Jpn. **69**, 2291 (2000).
  - <sup>17</sup> G. S. Uhrig and H. J. Schulz, Phys. Rev. B **54**, R9624 (1996).
  - <sup>18</sup> G. Bouzerar, A. P. Kampf, and G. I. Japaridze, Phys. Rev. B **58**, 3117 (1998).
  - <sup>19</sup> W. Zheng, C. J. Hamer, R. R. P. Singh, S. Trebst, and H. Monien, Phys. Rev. B **63**, 144411 (2001).
  - <sup>20</sup> I. Dzhyaloshinskii, J. Phys. Chem. Solids **4**, 241 (1958).
  - <sup>21</sup> T. Moriya, Phys. Rev. **120**, 91 (1960).
  - <sup>22</sup> L. Shekhtman, O. Entin-Wohlman, and A. Aharony, Phys. Rev. Lett. **69**, 836 (1992).
  - <sup>23</sup> L. Shekhtman, A. Aharony, and O. Entin-Wohlman, Phys. Rev. B **47**, 174 (1993).
  - <sup>24</sup> T. Sakai, O. Cépas, and T. Ziman, J. Phys. Soc. Jpn. **69**, 3521 (2000).
  - <sup>25</sup> O. Cépas, K. Kakurai, L. P. Regnault, T. Ziman, J. P. Boucher, N. Aso, M. Nishi, H. Kageyama, and Y. Ueda, Phys. Rev. Lett. **87**, 167205 (2001).
  - <sup>26</sup> O. Cépas, T. Sakai, and T. Ziman, Prog. Theor. Phys. Suppl. **145**, 43 (2002).
  - <sup>27</sup> R. K. Kremer, I. Loa, F. S. Razavi, and K. Syassen, Solid state comm. **113**, 217 (1999).
  - <sup>28</sup> Martin-Puplett spectrometer SPS-200 is made by Sciencetech Inc., Ontario, Canada.
  - <sup>29</sup> A. I. Smirnov, M. N. Popova, A. B. Sushkov, S. A. Golubchik, D. I. Khomskii, M. V. Mostovoy, A. N. Vasilev, M. Isobe, and Y. Ueda, Phys. Rev. B **59**, 14546 (1999).
  - <sup>30</sup> M. Poirier, P. Fertey, J. Jegoudez, and A. Revcolevschi, Phys. Rev. B **60**, 7341 (1999).
  - <sup>31</sup> A. Damascelli, C. Presura, D. van der Marel, J. Jegoudez, and A. Revcolevschi, Phys. Rev. B **61**, 2535 (2000).
  - <sup>32</sup> M. N. Popova, A. B. Sushkov, S. A. Klimin, E. P. Chukalina, B. Z. Malkin, M. Isobe, and Y. Ueda, Phys. Rev. B **65**, 144303 (2002).
  - <sup>33</sup> D. Smirnov, J. Leotin, P. Millet, J. Jegoudez, and A. Revcolevschi, Physica B **259-261**, 992 (1999).
  - <sup>34</sup> F. Keffer, Phys. Rev. **126**, 896 (1962).
  - <sup>35</sup> M. Lohmann, H. A. Krug von Nidda, M. V. Eremin, A. Loidl, G. Obermeier, and S. Horn, Phys. Rev. Lett. **85**, 1742 (2000).
  - <sup>36</sup> Z. V. Popović, M. J. Konstantinović, R. Gajić, V. N. Popov, M. Isobe, Y. Ueda, and V. V. Moshchalkov, Phys. Rev. B **65**, 184303 (2002).
  - <sup>37</sup> R. Loudon, *The Quantum Theory of Light* (Oxford University Press, London - New York - Toronto, 1983), 2nd ed.
  - <sup>38</sup> B. D. Gaulin, M. D. Lumsden, R. K. Kremer, M. A. Lumsden, and H. Dabkowska, Phys. Rev. Lett. **84**, 3446 (2000).
  - <sup>39</sup> P. Fertey, M. Poirier, M. Castonguay, J. Jegoudez, and A. Revcolevschi, Phys. Rev. B **57**, 13698 (1998).
  - <sup>40</sup> M. Azzouz and C. Bourbonnais, Phys. Rev. B **53**, 5090 (1996).
  - <sup>41</sup> K. Takehana, T. Takamasu, G. Kido, M. Isobe, and Y. Ueda, Physica B **294-295**, 79 (2001).
  - <sup>42</sup> P. Lemmens, M. Fischer, G. Els, G. Güntherodt, A. S. Mischenko, M. Weiden, R. Hauptmann, C. Geibel, and F. Steglich, Phys. Rev. B **58**, 14159 (1998).
  - <sup>43</sup> M. J. Konstantinović, J. C. Irwin, M. Isobe, and Y. Ueda,

- Phys. Rev. B **65**, 012404 (2001).
- <sup>44</sup> M. Isobe and Y. Ueda, J. Magnetism and Magnetic Materials **177-181**, 671 (1998).
- <sup>45</sup> G. Blumberg, A. Gozar, B. S. Dennis, R. K. Kremer, P. Canfield, and A. F. Panchula, private communication, not published.
- <sup>46</sup> I. Loa, K. Syassen, R. K. Kremer, U. Schwarz, and M. Hanfland, Phys. Rev. B **60**, R6945 (1999).
- <sup>47</sup> K. Ohwada, Y. Fujii, N. Takusue, M. Isobe, Y. Ueda, H. Nakao, Y. Wakabayashi, Y. Murakami, K. Ito, Y. Amemiya, et al., Phys. Rev. Lett. **87**, 086402 (2001).
- <sup>48</sup> H. Schwenk, S. Zherlitsyn, B. Luthi, E. Morre, and C. Geibel, Phys. Rev. B **60**, 9194 (1999).
- <sup>49</sup> G. Breit and E. Wigner, Phys. Rev. **49**, 519 (1936).
- <sup>50</sup> U. Fano, Phys. Rev. **124**, 1866 (1961).
- <sup>51</sup> C. C. Homes, T. Timusk, D. A. Bonn, R. Liang, and W. N. Hardy, Can. J. Phys. **73**, 663 (1995).
- <sup>52</sup> It has been shown by Damascelli *et al.*<sup>31</sup> that the direct two-magnon optical absorption is possible because of the asymmetrical charge distribution on the ladder rungs.